DE-FG05-80ET-53088-694 IFSR #694

Stabilization of the Resistive Shell Mode in Tokamaks

RICHARD FITZPATRICK and AHMET AYDEMIR
Institute for Fusion Studies
The University of Texas at Austin
Austin, Texas 78712

February 1995

Stabilization of the Resistive Shell Mode in Tokamaks

Richard Fitzpatrick & Ahmet Aydemir

Institute for Fusion Studies, The University of Texas at Austin

Austin, Texas 78712

February 10, 1995

Abstract

The stability of current-driven external-kink modes is investigated in a tokamak plasma surrounded by an external shell of finite electrical conductivity. According to conventional theory, the ideal mode can be stabilized by placing the shell sufficiently close to the plasma, but the non-rotating "resistive shell mode," which grows on the characteristic L/R time of the shell, always persists. It is demonstrated, using both analytic and numerical techniques, that a combination of strong edge plasma rotation and dissipation somewhere inside the plasma is capable of stabilizing the resistive shell mode. This stabilization mechanism does not necessarily depend on toroidicity or the presence of resonant surfaces inside the plasma.

1 INTRODUCTION

The ideal stability of current-driven helical magnetic perturbations in a large aspect-ratio toroidal pinch device (e.g. a tokamak) was first investigated by Newcomb [1]. The stability of a general mode is governed by the marginally-stable equations of ideal magnetohydrodynamics (MHD), which reduce to

$$\mathcal{L}\psi = 0, \tag{1}$$

where $\psi(r)$ is the perturbed poloidal flux eigenfunction, r the minor radius of flux-surfaces, and $\mathcal{L}$ the Euler-Lagrange operator which minimizes the well-known ideal-MHD quantity δW [2]. External-kink modes are of primary importance when there are no resonant surfaces (i.e. no flux-surfaces on which the wave-number of the perturbation parallel to the equilibrium magnetic field is zero) located inside the plasma. For the moment, it is assumed that the plasma is surrounded by a vacuum region which extends to infinity. The stability of the ideal external-kink mode can be determined via a simple test. A well-behaved eigenfunction is launched from the magnetic axis ($r = 0$) and evolved according to Eq. (1). If the eigenfunction keeps the same sign all the way out to $r = \infty$ then the external-kink mode is stable. On the other hand, if the eigenfunction crosses zero at finite r then the mode is unstable. This criterion is illustrated in Fig. 1.

Suppose that the plasma is surrounded by a concentric perfectly conducting shell of minor radius $r_{\rm w}$. The physical boundary condition at the shell is $\psi(r_{\rm w}) = 0$. In this case, Newcomb's criterion is somewhat modified. A well-behaved eigenfunction is launched from the magnetic axis, as before, but the eigenfunction must now cross zero before reaching the shell in order for the ideal external-kink mode to be unstable. This criterion is illustrated in Fig. 2. In general, the modified instability criterion is harder to satisfy than Newcomb's original criterion. Indeed, it can be demonstrated that a perfectly conducting shell placed

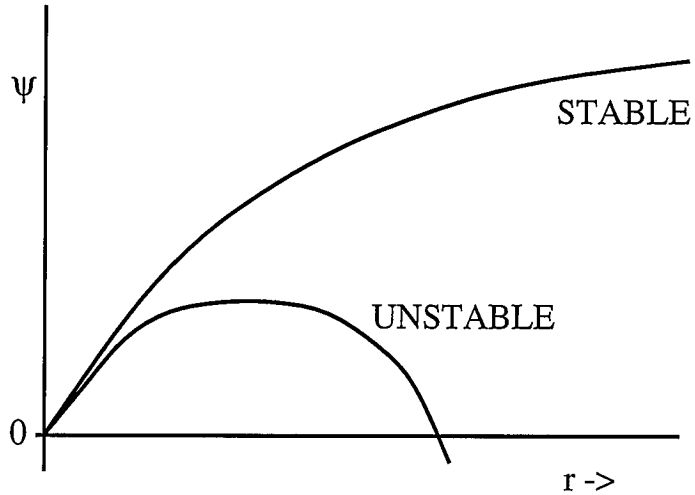

Figure 1: Illustration of Newcomb's stability criterion for ideal external-kink modes in a large aspect-ratio toroidal pinch plasma surrounded by a vacuum region which extends to infinity

right at the edge of the plasma is proof against any external-kink mode [3].

Consider a plasma equilibrium which is unstable to an external-kink mode in the absence of a conducting shell. The well-behaved eigenfunction launched from the magnetic axis crosses zero at some radius r_c outside the plasma [see Fig. 2]. According to the modified instability criterion, the ideal mode can be stabilized by placing a perfectly conducting shell at any radius $r_{\rm w} < r_c$. Clearly, those operational stability boundaries of a toroidal pinch device which are set by external-kink modes can be substantially improved by surrounding the plasma by a perfectly conducting shell. The optimum configuration is to have the shell as close as possible to the edge of the plasma.

In most tokamaks the role of the shell is played by the vacuum vessel. Real vacuum vessels are made out of conducting material but are by no means *perfect* conductors. In fact, magnetic flux diffuses through them on a characteristic L/R time, denoted $\tau_{\rm w}$. This time-scale is invariably very much less than the pulse length of the device. Thus, a real vacuum vessel cannot maintain the ideal constraint $\psi(r_{\rm w}) = 0$ for any significant length of time. According to conventional theory, a resistive vacuum vessel placed inside the critical

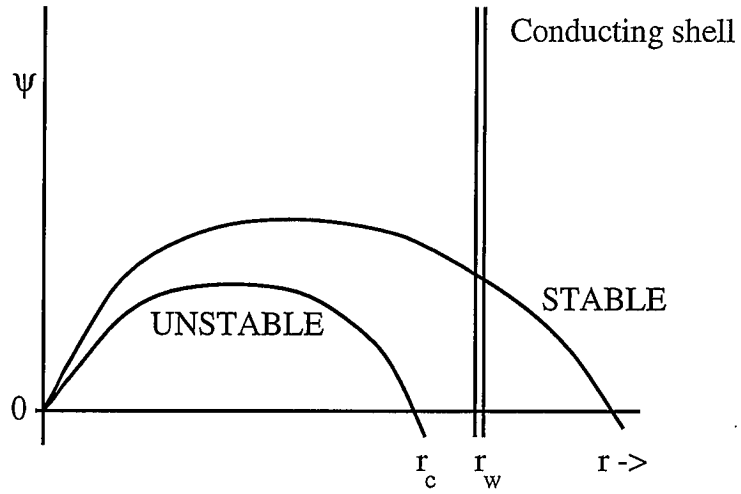

radius r_c converts the ideal external-kink mode into a non-rotating resistive mode which grows on the characteristic L/R time of the vessel. This mode is usually referred to as the resistive shell mode. The (very) approximate dispersion relation for the resistive shell mode is (see Section 2)

$$\gamma\tau_{\rm w} \simeq \frac{a}{r_c - r_{\rm w}}. \tag{2}$$

Here, γ is the growth-rate and a is the minor radius of the plasma. The growth-rate of the resistive mode connects smoothly with that of the ideal mode as $r_{\rm w} \rightarrow r_c$. For $r_{\rm w} > r_c$ the ideal mode is unstable. According to a well-established and widely quoted result, if the ideal mode is unstable in the absence of an ideal conducting shell then there is always an instability (either an ideal external-kink mode or a resistive shell mode) in the presence of a resistive conducting shell [4]. Thus, a real vacuum vessel is predicted to have no effect whatsoever on those operational stability boundaries of a tokamak plasma which are set by external-kink modes.

The most unambiguous observations of the resistive shell mode come from Reversed Field Pinches (RFPs). RFPs are high current, short pulse toroidal pinch devices which are unstable

to a wide spectrum of external-kink modes [5]. RFPs are conventionally surrounded by a thick close-fitting conducting shell whose L/R time is much longer than the pulse duration. This ensures stability against external-kink modes. However, in a number of experiments the thick shell was replaced by a thin shell whose L/R time was much less than the pulse length. In HBTX-1C non-rotating instabilities were observed growing on the characteristic L/R time of the shell. These instabilities lead to the premature termination of the discharge after a few L/R times. The spectrum and growth-rates of the non-rotating instabilities agreed very well with those predicted for the resistive shell mode [6]. Similar non-rotating instabilities were observed on OHTE, but these did not necessarily give rise to premature termination of the discharge [7]. Resistive shell modes were also observed on the REVERSATRON II device [8]. The conclusions drawn from the RFP "thin shell" experiments are that the resistive shell mode is a real and potentially very dangerous instability. These experiments stimulated many theoretical investigations. All concluded, after examining a variety of physical effects, that the resistive shell mode could *not* be stabilized [9–12].

In tokamak plasmas pressure-driven external-kink modes often limit the maximum achievable β. Here, $\beta = 2\mu_0 < p > / < B^2 >$, where $< \cdots >$ denotes a volume average, is a measure of the plasma pressure. Tokamak β limits are conventionally expressed in terms of $\beta_N = \beta/(I_p[\mathrm{MA}]/a[\mathrm{m}]B_0[\mathrm{T}])$, where I_p is the toroidal plasma current and B_0 is the on-axis toroidal magnetic field-strength. Theoretical studies with optimized plasma profiles and no conducting shell predict β limits of $\beta_N \lesssim 3.5$ [13]. However, the DIII-D tokamak routinely produces plasmas with $\beta_N \lesssim 5$ [14]. These enhanced performance plasmas are stable for many L/R times of the vacuum vessel. In fact, the experimental β limits agree quite well with those predicted by theory when the plasma is surrounded by a perfectly conducting shell placed at about the position of the DIII-D vacuum vessel [15]. This result implies that the resistive shell mode is *stable* in DIII-D. Similar conclusions have been drawn from experiments performed on the PBX-M [16] and HBT-EP [17] tokamaks.

Advanced tokamak designs aim to simultaneously maximize the fusion reactivity (i.e. the plasma β) and the non-inductive bootstrap current [18]. The eventual aim is, of course, to design a steady-state fusion reactor in which all of the toroidal current is maintained in the plasma by non-inductive means. The β limits in advanced tokamak designs are invariably set by low mode-number external-kink modes. Acceptable β limits are only achievable if the stabilizing effect of a close-fitting conducting shell is taken into account in the MHD calculations [19]. Of course, this effect is only realizable if the resistive shell mode is stabilized. Thus, advanced tokamaks are currently being designed on the premise that *the resistive shell mode is stable.* This is a worrying state of affairs given the RFP experimental results and the previous inability of MHD theorists to find any stabilization mechanism whatsoever for the resistive shell mode. Fortunately, however, a possible stabilization mechanism for this mode has recently been discovered [20].

The majority of present day tokamaks achieve high-β by heating the plasma with unbalanced neutral beam injection (NBI). Thus, there is a strong tendency for high-β plasmas to also be rapidly rotating plasmas. The typical toroidal rotation frequency in NBI plasmas is about 10 kHz [21]. Numerical [20] and analytic [22] studies have recently demonstrated that it is possible to stabilize the resistive shell mode by a combination of strong plasma rotation and sound wave absorption at a toroidally coupled sideband rational surface located inside the plasma. The required levels of rotation are typically about 5% of the Alfvén frequency. This stabilization mechanism depends on strong rotation, toroidicity, plasma compressibility, and the presence of at least one resonant surface in the plasma. However, more recent numerical work has established that the resistive shell mode can be stabilized by a combination of strong plasma rotation and viscosity in a cylindrical incompressible plasma [23].

The aim of this paper is to establish the minimum set of requirements for the stabilization of the resistive shell mode in a rotating tokamak plasma. In particular, we hope to discover what physics determines the critical rotation rate needed to stabilize the mode, whether some

form of plasma dissipation (e.g. absorption of sound waves, viscosity) is always required for stabilization, and what the optimum properties of the conducting shell are for achieving stabilization at low plasma rotation rates. An analytic model based on reduced-MHD in cylindrical geometry is presented in Section 2. The predictions of this model are compared with numerical simulations in Section 3. The analytic model is extended in Sections 4, 5, and 6. The conclusions of our investigations are given in Section 7.

2 AN ANALYTIC MODEL

2.1 Basic Scenario

Consider a conventional large aspect-ratio, low β, circular flux-surface, tokamak equilibrium. The linearized, incompressible, non-ideal (i.e. including the effects of plasma inertia, resistivity, and viscosity) equations of reduced-magnetohydrodynamics (reduced-MHD) are used to investigate the stability of a general m/n (m is the poloidal mode-number, and n the toroidal mode-number) current-driven external-kink mode in the presence of plasma rotation and a thin resistive vacuum vessel. The basic scenario is illustrated in Fig. 3. The region between the edge of the main, current carrying plasma and the vacuum vessel, which in reality is filled with a cold tenuous plasma, is treated as an "effective vacuum": i.e. a plasma with negligible inertia and viscosity, and very high resistivity. An inertial layer forms in the outer regions of the current carrying plasma in order to moderate the growth of the external-kink mode. A much thinner "skin current" layer forms on the outer edge of the inertial layer. The aim of this investigation is to establish whether or not plasma rotation can lead to stabilization of the non-rotating resistive shell mode branch of the external-kink dispersion relation.

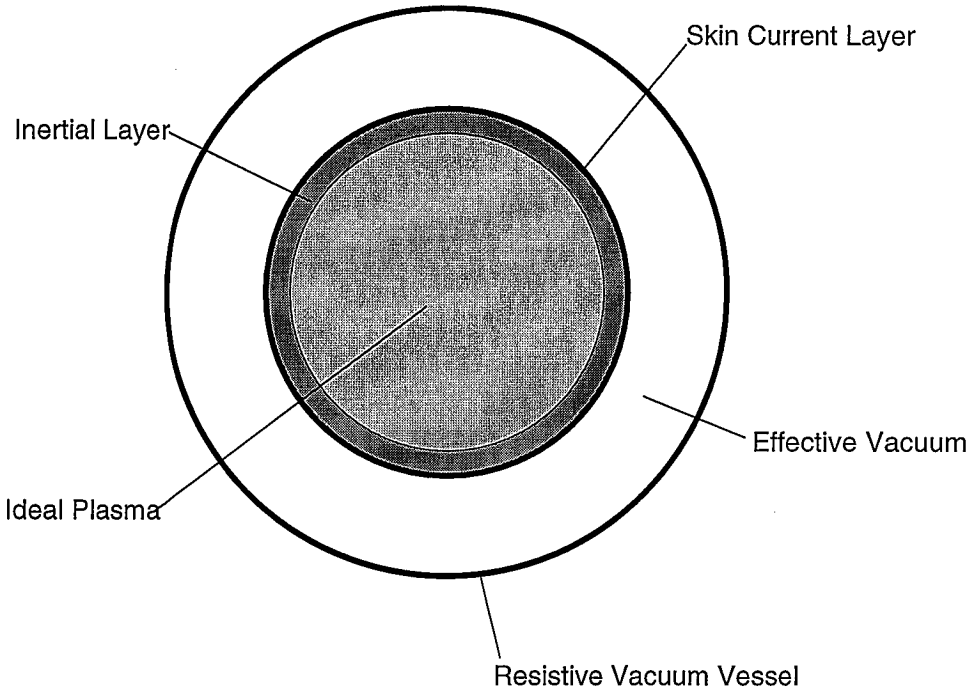

Figure 3: A poloidal cross-section of the plasma illustrating the basic scenario of the analytic model

2.2 Reduced Magnetohydrodynamics

2.2.1 Equilibrium

The standard right-handed cylindrical polar coordinates (r, θ, z) are employed. The plasma is assumed to be periodic in the z-direction with periodicity length $2\pi R_0$, where R_0 is the simulated major radius. The equilibrium magnetic field is written

$$\mathbf{B} \simeq (0, B_\theta(r), B_z). \tag{3}$$

The basic large aspect-ratio, low-β ordering scheme takes the form

$$\frac{B_\theta}{B_z} \sim \epsilon \equiv \frac{a}{R_0} \ll 1, \tag{4}$$

with

$$\frac{\mu_0 r p'}{{B_z}^2} \sim \epsilon^2. \tag{5}$$

Here, a is the minor radius of the current carrying plasma, $p(r)$ is the plasma pressure, and $'$ denotes $\partial/\partial r$. The "safety-factor" is defined

$$q(r) = \frac{r B_z}{R_0 B_\theta}. \tag{6}$$

Finally, the equilibrium "toroidal" current is given by

$$\mu_0 j_z(r) \simeq \frac{1}{r}\frac{d}{dr}(r B_\theta) = \frac{B_z}{R_0}\frac{1}{r}\frac{d}{dr}\left(\frac{r^2}{q}\right). \tag{7}$$

2.2.2 Linear Stability

The two equations to be analyzed correspond to linearized force balance,

$$\rho\frac{\partial \mathbf{v}}{\partial t} = \delta j \wedge \mathbf{B} + \mathbf{j} \wedge \delta B - \nabla \delta p + \mathbf{F}_\mu, \tag{8}$$

and the linearized Ohm's law

$$\delta E + \mathbf{v} \wedge \mathbf{B} = \eta\, \delta j. \tag{9}$$

Here, $\mathbf{v}$, δp, δB, δE, and δj are the perturbed plasma velocity, pressure, magnetic field, electric field, and current density, respectively, and $\partial/\partial t$ is the time derivative in the plasma frame. The θ and z components of the perturbed viscous force density are

$$F_{\mu\theta} \simeq \frac{1}{r^2}\frac{\partial}{\partial r}\mu_\perp r^3 \frac{\partial}{\partial r}\frac{v_\theta}{r} - \frac{m^2}{r^2}\mu_\perp v_\theta + 2\mathrm{i}\frac{m}{r}\mu_\perp v_r, \tag{10a}$$

$$F_{\mu z} \simeq \frac{1}{r}\frac{\partial}{\partial r}\mu_\perp r \frac{\partial}{\partial r} v_z - \frac{m^2}{r^2}\mu_\perp v_z, \tag{10b}$$

where an $\exp[\mathrm{i}\,(m\theta - nz/R_0)]$ dependence of perturbed quantities is assumed. In the above, $\rho(r)$ is the plasma mass density, $\eta(r)$ the parallel electrical conductivity, and $\mu_\perp(r)$ the (anomalous) perpendicular viscosity. Note that the effects of centrifugal forces and radial shear in the equilibrium plasma rotation profile are neglected in Eq. (8).

The perturbed magnetic field is written in terms of a poloidal flux function,

$$\delta B = \nabla\psi \wedge \hat{\mathbf{z}}, \tag{11}$$

and the perturbed plasma velocity is written in terms of a displacement stream function,

$$\mathbf{v} = \mathrm{i}\gamma_0 \nabla\widehat{\phi} \wedge \widehat{\mathbf{z}}, \tag{12}$$

assuming an $\exp(\gamma_0 t)$ time dependence of perturbed quantities in the plasma frame of reference (which corresponds to the $\mathbf{E} \wedge \mathbf{B}$ frame in reduced-MHD).

The linearized reduced-MHD equations can be written

$$\frac{\eta}{\mu_0}\nabla^2\psi = \gamma_0\,(\psi - F\widehat{\phi}), \tag{13a}$$

$$\frac{F}{\mu_0}\nabla^2\psi + \frac{m}{r}\,j_z'\,\psi = -{\gamma_0}^2\,{\nabla_\rho}^2\widehat{\phi} + \gamma_0\,{\nabla_\mu}^4\widehat{\phi}, \tag{13b}$$

where

$$F = \frac{n}{R_0}B_z - \frac{m}{r}B_\theta, \tag{14}$$

and

$${\nabla_\rho}^2(\cdots) \equiv \frac{1}{r}\frac{\partial}{\partial r}\,\rho r\,\frac{\partial}{\partial r}(\cdots) - \frac{m^2}{r^2}\,\rho\,(\cdots), \tag{15a}$$

$$\begin{aligned}{\nabla_\mu}^4(\cdots) \equiv \frac{1}{r}\frac{\partial}{\partial r}\frac{1}{r}\Bigg\{&\frac{\partial}{\partial r}\,\mu_\perp r^3\,\frac{\partial}{\partial r}\frac{1}{r}\frac{\partial}{\partial r}\,(\cdots) - m^2\mu_\perp\frac{\partial}{\partial r}\,(\cdots)\\ &+2\,\frac{m^2}{r}\mu_\perp\,(\cdots)\Bigg\}.\end{aligned} \tag{15b}$$

2.2.3 Matching Conditions

Suppose that the plasma density, resistivity, and viscosity change abruptly at some boundary located at minor radius $r = b$ (e.g. the limiter radius). The four obvious matching conditions are

$$\psi(b_-) = \psi(b_+), \tag{16a}$$

$$\psi'(b_-) = \psi'(b_+), \tag{16b}$$

$$\widehat{\phi}(b_-) = \widehat{\phi}(b_+), \tag{16c}$$

$$\widehat{\phi}'(b_-) = \widehat{\phi}'(b_+). \tag{16d}$$

These correspond to the continuity of the radial magnetic field, the absence of an unresolved current sheet at $r = b$, continuity of the radial plasma displacement, and continuity of the tangential displacement, respectively.

The fifth matching condition is obtained by integrating the θ-component of Eq. (8) across the boundary:

$$\mu_\perp(b_-)\widehat{\phi}''(b_-) = \mu_\perp(b_+)\widehat{\phi}''(b_+). \tag{17}$$

This corresponds to the continuity of the viscous momentum flux across $r = b$. The sixth, and final, matching condition is obtained by integrating Eq. (13b) across the boundary:

$$\left[j_z \frac{m}{r}\psi + {\gamma_0}^2 \rho\, \widehat{\phi}' - \mathrm{i}\, F_{\mu\theta} \right]_{b_-}^{b_+} = 0. \tag{18}$$

The θ-component of Eq. (8) can be written

$$j_z \frac{m}{r}\psi + {\gamma_0}^2 \rho\, \widehat{\phi}' - \mathrm{i}\, F_{\mu\theta} - \frac{m}{r}\,\delta p = 0. \tag{19}$$

It is clear that the sixth matching condition ensures that the perturbed pressure δp is not discontinuous at $r = b$.

According to the above matching conditions the boundary between the two plasma regions does not necessarily lie on a magnetic flux surface. This implies that, in general, the perturbed current at $r = b$ is non-zero. It is only possible for this to be the case if

$$|\gamma_0| \gg |k_\parallel c_s| \tag{20}$$

in the vicinity of $r = b$, where $k_\parallel = -F/B_z$ and c_s is the slower sound speed. This condition ensures that parallel flows are not fast enough to force the boundary to lie on a magnetic

surface. If

$$|\gamma_0| \ll |k_\parallel c_s| \tag{21}$$

in the vicinity of $r = b$ then the sixth matching condition is replaced by the ideal-MHD constraint

$$\left[\psi - F\widehat{\phi}\right]_{r=b} = 0. \tag{22}$$

This also implies, from Ohm's law Eq. (13a), that the perturbed current,

$$\mu_0 \delta \mathbf{j} \simeq -\nabla^2 \psi \, \widehat{\mathbf{z}}, \tag{23}$$

is zero at the boundary.

Consider the special case where the region $r > b$ is an "effective vacuum": i.e. a plasma with negligible inertia and viscosity, and very high resistivity. If the perturbed motion at the edge is supersonic, so that $|\gamma_0| \gg |k_\parallel c_s|$ where c_s is the sound speed in the low temperature effective vacuum, then the fifth and sixth matching conditions reduce to

$$\widehat{\phi}''(b_-) = 0, \tag{24}$$

and

$$\left[j_z \frac{m}{r}\psi + {\gamma_0}^2 \rho \widehat{\phi}' - \mathrm{i}\, F_{\mu\theta}\right]_{r=b_-} = 0, \tag{25}$$

respectively.

2.3 The Ideal-MHD Region

In the main, current carrying plasma (outer radius $r = a$) the perturbation is governed by the marginally-stable ideal-MHD equations (i.e. the reduced-MHD equations in the limit where plasma inertia, resistivity, and viscosity are negligible) except for a relatively thin region close to the edge where plasma inertia becomes important. The marginally-stable ideal-MHD equations are written

$$\psi - F\,\widehat{\phi} \;=\; 0, \tag{26a}$$

$$\frac{F}{\mu_0}\nabla^2\psi + \frac{m}{r}j_z'\psi = 0. \tag{26b}$$

The m/n mode rational surface (radius r_s, where $q(r_s) = m/n$) is assumed to lie outside the current carrying plasma (i.e. $r_s > a$). This is justified because current-driven external-kink modes are only unstable when this is the case [24]. Equation (26b) can be integrated out from the magnetic axis ($r = 0$) to a radius just inside the inertial layer (radius a_-, say). This yields $\psi(r)$ in the region $r < a_-$ (the solution is assumed to be well behaved in the vicinity of the magnetic axis). Close to the inertial layer

$$\psi(r) \simeq \Psi_{a_-}\left(1 - \frac{r - a_-}{d_c\, a_-}\right). \tag{27}$$

The parameter

$$\frac{1}{d_c} = -\, r\frac{\partial\psi}{\partial r}\Big/\psi\,\Big|_{r=a_-} \tag{28}$$

controls the stability of the external-kink mode.

2.4 The Edge Region

2.4.1 Layer Equations

The edge region, comprising the inertial layer and the "skin current" layer, is assumed to be relatively thin compared to the plasma minor radius. It follows that the radial length-scale of perturbed quantities in the edge region is small compared to that of equilibrium quantities. Under these circumstances the reduced-MHD equations can be written as a pair of layer equations:

$$\frac{\partial^2\psi}{\partial x^2} \simeq g S_c\,[\psi - (x-1)\phi]\,, \tag{29a}$$

$$(x-1)\frac{\partial^2\psi}{\partial x^2} \simeq -g^2\frac{\partial\phi^2}{\partial x^2} + g\nu_c\frac{\partial^4\phi}{\partial x^4}, \tag{29b}$$

where $F = (n/R_0)\,B_z - (m/r)\,B_\theta$ is expanded linearly about $r = a$. In the layer equations:

$$x = \frac{r-a}{c\,a}, \tag{30a}$$

$$c = \frac{m/n - q_a}{s_a\,q_a} \simeq \frac{r_s - a}{a}, \tag{30b}$$

$$q_a = q(a), \tag{30c}$$

$$s_a = \frac{r}{q}\,\frac{dq}{dr}\bigg|_{r=a}, \tag{30d}$$

$$\phi = c\,n s_a \frac{B_z}{R_0}\,\widehat{\phi}, \tag{30e}$$

$$g = \frac{\gamma_0\,\tau_A}{c\,n s_a}, \tag{30f}$$

$$S_c = c^3\,n s_a\,\frac{\tau_R}{\tau_A}, \tag{30g}$$

$$\nu_c = \frac{\tau_A}{\tau_V}\bigg/\,(c^3\,n s_a), \tag{30h}$$

$$\tau_A = \frac{R_0}{B_z}\sqrt{\mu_0 \rho(a)}, \tag{30i}$$

$$\tau_R = \frac{\mu_0 a^2}{\eta(a)}, \tag{30j}$$

$$\tau_V = \frac{a^2 \rho(a)}{\mu_\perp(a)}. \tag{30k}$$

In addition,

$$\gamma_0 = \gamma + \mathrm{i}\,\omega_0, \tag{31}$$

where $\omega_0 = m\Omega_\theta - n\Omega_z$. Here, γ is the mode growth-rate in the frame of the resistive vacuum vessel (i.e. the laboratory frame) whilst Ω_θ and Ω_z are, respectively, the poloidal and "toroidal" angular rotation velocities of the edge plasma.

The parameter c is essentially the normalized (with respect to the minor radius a) distance of the rational surface from the edge of the current carrying plasma. The scaled radial variable x is defined such that the edge of the plasma lies at $x = 0$ and the mode rational surface at $x = 1$. The parameter g is the normalized mode growth-rate in the rotating frame of the edge plasma. The parameters S_c and ν_c characterize the plasma resistivity and viscosity, respectively, in the edge region. Finally, the quantities τ_A, τ_R, and τ_V are, respectively, the typical Alfvén, resistive, and viscous time-scales of the edge plasma.

2.4.2 The Inertial Layer

The radial variation length-scale of the inertial layer is the distance from the edge of the current carrying plasma to the mode rational surface; i.e. $c\,a$. This length-scale is assumed to be much smaller than the plasma minor radius, which implies that $c \ll 1$. Thus, the concept of a thin inertial layer is only valid when the rational surface lies relatively close to the plasma. If this is the case then the layer equations reduce to

$$\psi_0 \simeq (x-1)\,\phi_0, \tag{32a}$$

$$(x-1)\,\frac{\partial^2\psi_0}{\partial x^2} \simeq -g^2\,\frac{\partial^2\phi_0}{\partial x^2}, \tag{32b}$$

where the neglect of viscosity and inertia are valid provided that $\nu_c \ll 1$ and $S_c \gg 1$, respectively. The above pair of equations can be combined to form a single equation

$$\frac{\partial}{\partial x}\left[\left\{(x-1)^2+g^2\right\}\frac{\partial\phi_0}{\partial x}\right] \simeq 0. \tag{33}$$

The solution of this equation which is consistent with the inner boundary condition Eq. (27) is

$$\phi_0(x) = -\Psi_{a-}(1-c/d_c)\int_{-\infty}^{x}\frac{dx}{(x-1)^2+g^2} - \Psi_{a-}\frac{c}{d_c}, \tag{34a}$$

$$\psi_0(x) = -\Psi_{a-}(1-c/d_c)\,(x-1)\int_{-\infty}^{x}\frac{dx}{(x-1)^2+g^2}$$

$$-\Psi_{a-}\frac{c}{d_c}\,(x-1), \tag{34b}$$

$$\mu_0\delta j_z(x) \;\simeq\; \Psi_{a-}(1-c/d_c)\,\frac{2g^2}{[(x-1)^2+g^2]^2}. \tag{34c}$$

Note that the perturbed current decays strongly into the plasma on the radial length-scale $c\,a$ [see Eq. (30b)]. This justifies the neglect of inertia and other non-ideal effects (which is equivalent to neglecting the perturbed current) throughout the bulk of the current carrying plasma (since $c \ll 1$).

The viscous and resistive corrections to the above solution are obtained by expanding the layer equations (29) to higher order in ν_c and ${S_c}^{-1}$. It is easily demonstrated that

$$[(x-1)^2+g^2]\phi_1' = g\nu_c\phi_0''' - \frac{1}{gS_c}\left\{[(x-1)^2\phi_0]''' - 4[(x-1)\phi_0]''\right\}, \tag{35}$$

where $'$ denotes $\partial/\partial x$. This yields

$$\begin{aligned}\phi_1(x) \;=\; & -\Psi_{a-}(1-c/d_c)\,g\nu_c\int_{-\infty}^{x}\left\{\frac{6}{[(x-1)^2+g^2]^3} - \frac{8g^2}{[(x-1)^2+g^2]^4}\right\}dx. \\ & -\Psi_{a-}(1-c/d_c)\frac{g}{S_c}\int_{-\infty}^{x}\left\{\frac{10}{[(x-1)^2+g^2]^3} - \frac{8g^2}{[(x-1)^2+g^2]^4}\right\}dx.\end{aligned} \tag{36}$$

It can also be shown that

$$\psi_1(x) = (x-1)\phi_1(x) - \Psi_{a-}(1-c/d_c)\frac{g}{S_c}\frac{2}{[(x-1)^2+g^2]^2}. \tag{37}$$

2.4.3 The "Skin Current" Layer

The "skin current" layer is situated on the outer edge of the inertial layer (i.e. at $x = 0$). It is assumed to be much thinner than the inertial layer, so in this region the layer equations reduce to

$$\frac{\partial^2\psi}{\partial x^2} \;\simeq\; gS_c[\psi+\phi], \tag{38a}$$

$$-\frac{\partial^2\psi}{\partial x^2} \simeq -g^2\frac{\partial\phi^2}{\partial x^2} + g\nu_c\frac{\partial^4\phi}{\partial x^4}. \tag{38b}$$

The complete solution in the edge region can be written

$$\phi(x) = \phi_0(x) + \phi_1(x) + \tilde{\phi}\exp(kx), \tag{39a}$$

$$\psi(x) = \psi_0(x) + \psi_1(x) + \tilde{\psi}\exp(kx), \tag{39b}$$

where $\tilde{\phi}$ and $\tilde{\psi}$ are constants. Thus,

$$\frac{\tilde{\psi}}{\tilde{\phi}} = \frac{gS_c}{k^2 - gS_c} = g^2 - g\nu_c\,k^2, \tag{40}$$

giving

$$k^4 - g\left(\frac{1}{\nu_c} + S_c\right)k^2 + (1+g^2)\frac{S_c}{\nu_c} = 0. \tag{41}$$

Only those roots of the above quartic with *positive* real parts correspond to physical solutions which decay into the plasma. There are two such roots, denoted k_+ and k_-, where

$$k_\pm^{\,2} = \frac{g}{2}\left(\frac{1}{\nu_c} + S_c\right) \pm \frac{1}{2}\sqrt{g^2\left(\frac{1}{\nu_c} - S_c\right)^2 - 4\frac{S_c}{\nu_c}}. \tag{42}$$

The "skin current" solutions are written

$$\tilde{\phi}\exp(kx) \rightarrow \tilde{\phi}_+\exp(k_+x) + \tilde{\phi}_-\exp(k_-x), \tag{43}$$

etc. The "skin current" layer is much thinner than the inertial layer provided $|k_\pm| \gg 1$, which is usually the case when $\nu_c \ll 1$ and $S_c \gg 1$.

2.4.4 The Edge Boundary Conditions

At radius $r = a$ the solution in the edge region must be matched to that in the effective vacuum region. The two nontrivial matching conditions [Eqs. (24) and (25)] reduce to

$$\left.\frac{\partial^2\phi}{\partial x^2}\right|_{x=0} = 0, \tag{44}$$

and

$$\left[-g^2\,\frac{\partial\phi}{\partial x}+g\nu_c\,\frac{\partial^3\phi}{\partial x^3}\right]_{x=0}=0, \tag{45}$$

where it is assumed that the edge "toroidal" current is zero (i.e. $j_z(a)=0$). The condition for the validity of the latter matching condition, namely Eq. (20), translates to

$$|g|\gg\sqrt{\beta_{\rm edge}}, \tag{46}$$

where

$$\beta_{\rm edge}=\frac{\mu_0\,\Gamma p(a_+)}{{B_z}^2}. \tag{47}$$

Here, Γ is the ratio of specific heats and $p(a_+)$ is the plasma pressure just outside the last closed flux-surface (i.e. in the scrape-off layer). Since $g\sim O(1)$ in a rotating plasma (see later) and $\beta_{\rm edge}\ll 1$, this condition is easily satisfied in a conventional tokamak.

Now, integration of the vorticity layer equation (29b) from the inner edge of the inertial layer ($x\rightarrow-\infty$) to the outer edge of the "skin current" layer ($x=0$) gives

$$\left[(x-1)\,\frac{\partial\psi}{\partial x}-\psi\right]_{x\rightarrow-\infty}^{x=0}=\left[-g^2\,\frac{\partial\phi}{\partial x}+g\nu_c\,\frac{\partial^3\phi}{\partial x^3}\right]_{x\rightarrow-\infty}^{x=0}. \tag{48}$$

Equations (34), (36), (37), (39) and the matching condition (45) allow the above expression to be reduced to

$$(k_+ +1)\,\overline{\psi}_+ +(k_- +1)\,\overline{\psi}_-\simeq\frac{g^2}{1+g^2}-g\nu_c\,\frac{(6-2g^2)}{(1+g^2)^4}+\frac{g}{S_c}\,\frac{g^2\,(10+2g^2)}{(1+g^2)^4}, \tag{49}$$

where

$$\widetilde{\psi}_\pm=\Psi_{a-}(1-c/d_c)\,\overline{\psi}_\pm. \tag{50}$$

Likewise, the matching condition (44) reduces to

$$\frac{({k_+}^2\,\overline{\psi}_+ +{k_-}^2\,\overline{\psi}_-)}{S_c\nu_c}-\frac{(1+g^2)}{g\nu_c}\,(\overline{\psi}_+ +\overline{\psi}_-)\;\simeq\;\frac{2}{(1+g^2)^2}+g\nu_c\frac{(36-28g^2)}{(1+g^2)^5}$$

$$+\frac{g}{S_c}\frac{(60-4g^2)}{(1+g^2)^5}, \tag{51}$$

where use has been made of Eqs. (40) and (41). Equations (49) and (51) can be solved simultaneously to give $\overline{\psi}_+$ and $\overline{\psi}_-$ as functions of the complex growth-rate g.

2.4.5 The Edge Dispersion Relation

All information about the edge region (as far as the asymptotic matching is concerned) is summed up in the complex parameter Δ_a, which is defined

$$\frac{\partial\psi}{\partial x}\Big/\psi\Big|_{x=0} = -\frac{c}{d_c} + c\Delta_a. \tag{52}$$

It is clear from Eqs. (28) and (30a) that $\Delta_a = 0$ when there is no gradient discontinuity in ψ across the edge region. It follows from Eqs. (34), (36), (37), (39), and (48) that

$$c\Delta_a = \frac{(1-c/d_c)^2\, D}{1-(1-c/d_c)\, D}, \tag{53}$$

where

$$D \simeq (1-I) - g\nu_c\, J + \frac{g\, K}{S_c} - (\overline{\psi}_+ + \overline{\psi}_-), \tag{54}$$

and

$$I = \int_1^\infty \frac{dy}{y^2+g^2}, \tag{55a}$$

$$J = \int_1^\infty \left\{\frac{6}{(y^2+g^2)^3} - \frac{8g^2}{(y^2+g^2)^4}\right\} dy, \tag{55b}$$

$$K = \frac{2}{(1+g^2)^2} - \int_1^\infty \left\{\frac{10}{(y^2+g^2)^3} - \frac{8g^2}{(y^2+g^2)^4}\right\} dy. \tag{55c}$$

The above integrals can also be written

$$I = \frac{1}{2\mathrm{i}\, g}\ln\left(\frac{1+\mathrm{i}\, g}{1-\mathrm{i}\, g}\right), \tag{56a}$$

$$J = \frac{15+g^4}{12(1+g^2)^3} + \frac{(1-g^2/3-I)}{4g^4}, \tag{56b}$$

$$K = \frac{3+24g^2+5g^4}{12(1+g^2)^3} + \frac{5(1-g^2/3-I)}{4g^4}. \tag{56c}$$

Equations (42), (49), (51), (53), (54), and (56) allow the parameter Δ_a to be evaluated as a function of the complex growth-rate g.

2.5 The Full Dispersion Relation

2.5.1 The External Region

The reduced-MHD equations yield

$$\nabla^2 \psi \simeq 0 \tag{57}$$

in the effective vacuum region (since it is too resistive to carry any significant plasma current). The above equation has the independent solutions $r^{\pm m}$. Thus, the most general form for ψ just outside the current carrying plasma is

$$\psi(r) = \Psi_a \frac{(r/r_{\rm w})^m - (r/r_{\rm w})^{-m}}{(a/r_{\rm w})^m - (a/r_{\rm w})^{-m}} + \Psi_{\rm w} \frac{(a/r)^m - (a/r)^{-m}}{(a/r_{\rm w})^m - (a/r_{\rm w})^{-m}} \tag{58}$$

for $a < r < r_{\rm w}$, where Ψ_a is the "edge flux," $\Psi_{\rm w}$ the "wall flux," and $r_{\rm w}$ the minor radius of the vacuum vessel. In the true vacuum region $r > r_{\rm w}$ the solution is

$$\psi(r) = \Psi_{\rm w} \left(\frac{r}{r_{\rm w}}\right)^{-m}. \tag{59}$$

Equations (52) and (58) imply that

$$r\frac{\partial \psi}{\partial r} \Big/ \psi \Big|_{r=a} = -m \frac{1 + (a/r_{\rm w})^{2m}}{1 - (a/r_{\rm w})^{2m}} + \frac{2m\,(a/r_{\rm w})^m}{1 - (a/r_{\rm w})^{2m}} \frac{\Psi_{\rm w}}{\Psi_a} = -\frac{1}{d_c} + \Delta_a. \tag{60}$$

2.5.2 The Vacuum Vessel

The dispersion relation for a thin, uniform, resistive vacuum vessel which is concentric with the plasma takes the form

$$\Delta_{\rm w} = \left[r\frac{\partial \psi}{\partial r} \Big/ \psi \right]_{r_{\rm w-}}^{r_{\rm w+}} = \gamma\, \tau_{\rm w}, \tag{61}$$

where

$$\tau_{\rm w} = \frac{\mu_0\, r_{\rm w} \delta_{\rm w}}{\eta_{\rm w}} \tag{62}$$

is the characteristic vessel time-constant, or L/R time. Here, $\delta_{\rm w}$ is the vessel thickness and $\eta_{\rm w}$ is its electrical resistivity. The above "thin shell" dispersion relation is valid provided

$$\frac{\delta_{\rm w}}{r_{\rm w}} \ll |\gamma|\, \tau_{\rm w} \ll \frac{r_{\rm w}}{\delta_{\rm w}}. \tag{63}$$

Equations (58) and (61) imply that

$$\Delta_{\rm w} = -\frac{2m}{1-(a/r_{\rm w})^{2m}} + \frac{2m\,(a/r_{\rm w})^m}{1-(a/r_{\rm w})^{2m}}\,\frac{\Psi_a}{\Psi_{\rm w}}. \tag{64}$$

2.5.3 The Dispersion Relation

It is helpful to define the quantity

$$d = \frac{1}{m}\,\frac{(r_{\rm w}/a)^{2m}-1}{(r_{\rm w}/a)^{2m}+1}. \tag{65}$$

For a close fitting vacuum vessel (i.e. $r_{\rm w} \rightarrow a$) d is just the fractional spacing of the vessel from the edge of the plasma (i.e. $r_{\rm w} \simeq a\,(1+d)$). The dispersion relation is obtained by combining Eqs. (60) and (64). It reduces to the surprisingly simple form,

$$\left(d\,\Delta_a(\gamma) + 1 - \frac{d}{d_c}\right)\,(\,d\,\Delta_{\rm w}(\gamma) + 1 + md\,) = 1-(md)^2, \tag{66}$$

when written in terms of d. Equation (66) describes how the perturbed currents flowing in the edge region of the plasma are coupled to those flowing in the vacuum vessel by the ideal-MHD eigenfunction in the "outer" region (i.e. everywhere apart from the edge region and the vacuum vessel). The currents flowing in the edge region are described by the parameter Δ_a. Those flowing in the vessel are described by $\Delta_{\rm w}$. The ideal-MHD eigenfunction is specified by just three parameters; d which determines the radius of the vacuum vessel, d_c which determines the critical vessel radius beyond which the ideal external-kink mode becomes unstable (see later), and the poloidal mode number m.

2.6 A Simplified Dispersion Relation

2.6.1 Derivation of the Dispersion Relation

In the limit

$$g^2 \ll \frac{4S_c\nu_c}{(1+S_c\nu_c)^2} \leq 1 \tag{67}$$

Eq. (40) yields

$$k_\pm^{\,2} \simeq \pm \mathrm{i}\sqrt{\frac{S_c}{\nu_c}}, \tag{68}$$

implying that the width of the "skin current" layer is determined by a combination of plasma resistivity and viscosity. In this limit Eq. (51) gives

$$\overline{\psi}_+ + \overline{\psi}_- \simeq -2g\nu_c, \tag{69}$$

and Eqs. (56) reduce to

$$I \simeq 1 - \frac{g^2}{3}, \tag{70a}$$

$$J \simeq \frac{6}{5} - \frac{26\,g^2}{7}, \tag{70b}$$

$$K \simeq \frac{10\,g^2}{7}. \tag{70c}$$

Finally, Eqs. (53) and (54) yield

$$c\Delta_a \simeq (1 - c/d_c)^2 \left(\frac{g^2}{3} + \frac{4}{5}\,g\nu_c\right) \tag{71}$$

to lowest order in g.

It is helpful to define

$$\widehat{\gamma} = \sqrt{\frac{d}{3c}}\,(1 - c/d_c)\,\mathrm{Re}(g) = \sqrt{\frac{d}{3c}}\,(1 - c/d_c)\,\gamma\tau_A \Big/ (c\,ns_a), \tag{72a}$$

$$\Omega_0 = \sqrt{\frac{d}{3c}}\,(1 - c/d_c)\,\mathrm{Im}(g) = \sqrt{\frac{d}{3c}}\,(1 - c/d_c)\,\omega_0\tau_A \Big/ (c\,ns_a). \tag{72b}$$

In terms of these variables

$$d\,\Delta_a \simeq (\widehat{\gamma} + \mathrm{i}\,\Omega_0)^2 + \nu_*\,(\widehat{\gamma} + \mathrm{i}\,\Omega_0), \tag{73}$$

where

$$\nu_* = \frac{4/5}{c\,ns_a}\sqrt{\frac{3d}{c}}\,(1 - c/d_c)\,\frac{\tau_A}{c^2\,\tau_V}. \tag{74}$$

Equation (61) can be written

$$d\,\Delta_{\rm w} = S_*\,\widehat{\gamma}, \tag{75}$$

where

$$S_* = c\,n\,s_a\,\sqrt{\frac{3c}{d}}\,\frac{d\,\tau_{\rm w}}{\tau_A}\Bigg/\,(1-c/d_c). \tag{76}$$

The simplified dispersion relation is obtained by substituting Eqs. (73) and (75) into Eq. (66):

$$\left((\widehat{\gamma}+{\rm i}\,\Omega_0)^2+\nu_*\,(\widehat{\gamma}+{\rm i}\,\Omega_0)+1-\frac{d}{d_c}\right)(\,S_*\,\widehat{\gamma}+1+m d\,)\simeq 1-(m d)^2. \tag{77}$$

It can be seen that when the inequality (67) is satisfied the dispersion relation reduces to a simple cubic in the complex normalized growth-rate, $\widehat{\gamma}$. The dispersion relation is characterized by just six parameters: the poloidal mode number m; the normalized edge plasma rotation Ω_0; the "spacing" d between the vacuum vessel and the edge of the current carrying plasma; the critical "spacing" d_c of the vacuum vessel beyond which the ideal external-kink mode is unstable (see later); S_*, which parameterizes the time-constant of the vacuum vessel; and ν_*, which measures viscous dissipation at the edge of the plasma. Normally, $S_* \gg 1$ because vessel time-constants are typically long compared to plasma Alfvén time-scales. Also, $\nu_* \ll 1$ in accordance with the ordering $\nu_c \ll 1$ used to derive the edge dispersion relation (73). The first bracket in Eq. (77) describes the edge region: the first term corresponds to plasma inertia acting in the thick inertial layer; the second term corresponds to viscous dissipation acting predominantly in the thin "skin current" layer (although there is a contribution from the inertial layer); the final terms describe the MHD free-energy available to drive the ideal external-kink mode. The second bracket describes the passive response of the vacuum vessel to time-varying external perturbations. Finally, the terms on the right-hand side describe the coupling of the helical currents flowing in the edge region to those flowing in the vacuum vessel. Note that the plasma resistivity does not

appear explicitly in the simplified dispersion relation, despite the fact that resistivity helps to determine the width of the "skin current" layer.

2.6.2 The Roots of the Dispersion Relation

Since the simplified dispersion relation is cubic it naturally possesses three roots; these are denoted Root1, Root2, and Root3. Assuming that $S_* \gg 1$ and $\nu_* \ll 1$, Root1 can be written

$$\widehat{\gamma} \simeq -\mathrm{i}\,\Omega_0\left\{1+\frac{1-(md)^2}{2S_*\sqrt{d/d_c-1}\,(d/d_c-1+{\Omega_0}^2)}\right\}$$

$$-\sqrt{d/d_c-1}\left\{1-\frac{1-(md)^2}{2S_*\sqrt{d/d_c-1}\,(d/d_c-1+{\Omega_0}^2)}\right\}-\frac{\nu_*}{2} \tag{78}$$

for $d > d_c$, and

$$\widehat{\gamma} \simeq -\mathrm{i}\left(\Omega_0+\sqrt{1-d/d_c}\right)-\frac{1-(md)^2}{2S_*\sqrt{1-d/d_c}\left(\Omega_0+\sqrt{1-d/d_c}\right)}-\frac{\nu_*}{2} \tag{79}$$

for $d < d_c$. Root2, which is closely related to Root1, becomes

$$\widehat{\gamma} \simeq -\mathrm{i}\,\Omega_0\left\{1-\frac{1-(md)^2}{2S_*\sqrt{d/d_c-1}\,(d/d_c-1+{\Omega_0}^2)}\right\}$$

$$+\sqrt{d/d_c-1}\left\{1+\frac{1-(md)^2}{2S_*\sqrt{d/d_c-1}\,(d/d_c-1+{\Omega_0}^2)}\right\}-\frac{\nu_*}{2} \tag{80}$$

for $d > d_c$, and

$$\widehat{\gamma} \simeq -\mathrm{i}\left(\Omega_0-\sqrt{1-d/d_c}\right)+\frac{1-(md)^2}{2S_*\sqrt{1-d/d_c}\left(\Omega_0-\sqrt{1-d/d_c}\right)}-\frac{\nu_*}{2} \tag{81}$$

for $d < d_c$. Finally, Root3 takes the form

$$\widehat{\gamma} \simeq -\mathrm{i}\,\Omega_0\,\frac{\nu_*(1-(md)^2)}{S_*(1-d/d_c-{\Omega_0}^2)^2}+\frac{(1-md_c)(1+md)\,d/d_c+(1+md)\,{\Omega_0}^2}{S_*(1-d/d_c-{\Omega_0}^2)}. \tag{82}$$

Root1 is uninteresting because it is always stable. The behavior of Root2 and Root3 for the case of zero plasma rotation (i.e. $\Omega_0 = 0$) is sketched in Fig. 4. It can be seen that

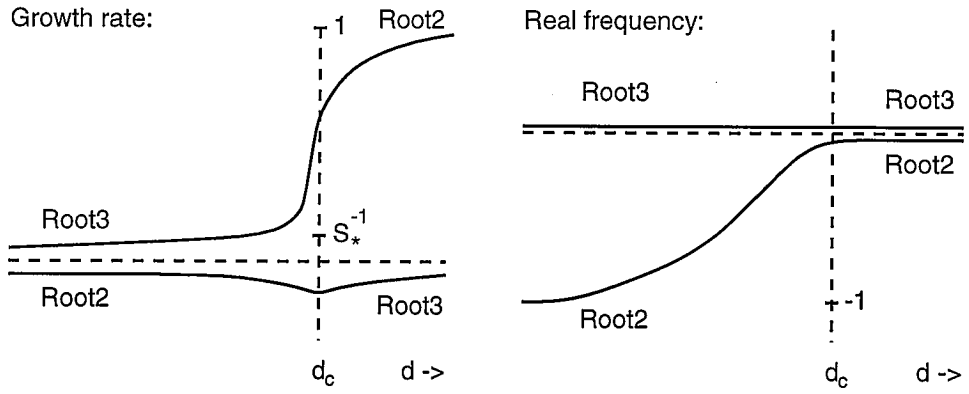

Figure 4: A schematic diagram showing the two non-trivial roots of the simplified dispersion relation (77) as functions of the vessel "spacing" d in the zero plasma rotation limit. The growth-rate is $\mathrm{Re}(\widehat{\gamma})$ and the real frequency is $-\mathrm{Im}(\widehat{\gamma})$. d_c is the critical vessel "spacing" for the stability of the ideal external-kink mode. Note that the two roots cross over when $d = d_c$.

for $d > d_c$ Root2 is an unstable, non-rotating mode with a typical external-kink growth-rate (i.e. $\widehat{\gamma} \sim O(1)$, which corresponds to $\gamma \sim k_\| v_A$, where $k_\|$ is the parallel wave-number at the plasma edge and v_A is the typical Alfvén velocity). For $d < d_c$, Root2 is a stable (but very close to marginality), negative frequency, external-kink mode (i.e. $|\widehat{\gamma}| \sim O(1)$). Root3 is non-rotating and possesses a typical resistive shell mode growth-rate (i.e. $\widehat{\gamma} \sim O(1/S_*)$, corresponding to $\gamma \sim O(1/\tau_\mathrm{w})$): it is stable for $d > d_c$ and unstable for $d < d_c$. The growth-rate of Root3 runs smoothly into that of Root2 as $d \rightarrow d_c$.

Root2 can be identified as the ideal external-kink mode and Root3 as the resistive shell mode. The ideal mode is only unstable for $d > d_c$, so d_c can be identified as the critical "spacing" of the vacuum vessel from the plasma required for ideal instability. According to Eq. (65), this translates to the following critical radius of the vacuum vessel:

$$\frac{r_c}{a} = \left(\frac{1 + m d_c}{1 - m d_c}\right)^{1/2m} . \tag{83}$$

So, the ideal mode is unstable for $r_\mathrm{w} > r_c$ and *vice versa*. The parameter d_c is determined by the plasma toroidal current profile via Eqs. (26) and (27). Note that in the absence of plasma rotation there is no position of the vacuum vessel (i.e. no value of r_w) for which

either the resistive shell mode or the ideal external-kink mode are not unstable. Thus, in the absence of rotation the presence of a *resistive* vacuum vessel does not modify the kink stability boundaries (i.e. if the kink mode is unstable in the absence of the vacuum vessel then there is always some corresponding mode which is unstable in the presence of the vessel).

The behavior of Root2 and Root3 for the case of a rotating plasma is sketched in Fig. 5. It can be seen that for $d > d_c$ the ideal external-kink mode (i.e. Root2) is unstable and co-rotates with the edge plasma (i.e. $-\mathrm{Im}(\hat{\gamma}) = \Omega_0$). For $d < d_0$, where

$$d_0 = d_c\,(1 - {\Omega_0}^2), \tag{84}$$

the resistive shell mode (i.e. Root3) is robustly unstable. In the "transition region" (i.e. $d_0 < d < d_c$) the resistive shell mode is robustly stable, and the kink mode takes the form of a positive frequency mode which is slipping backwards with respect to the edge plasma (i.e. $0 < -\mathrm{Im}(\hat{\gamma}) < \Omega_0$) and is close to marginality. The latter mode is destabilized by the finite resistivity of the vacuum vessel but stabilized by viscous dissipation at the edge of the plasma. According to Eqs. (81) and (82), the criterion for the stability of the kink and resistive shell modes when $d < d_c$ (i.e. when the ideal kink mode is stabilized by the vacuum vessel) is given by

$$\Omega_0 > \sqrt{1 - d/d_c} + \frac{1 - (md)^2}{S_*\nu_*\sqrt{1 - d/d_c}}. \tag{85}$$

Clearly, it is possible to stabilize both modes when $d < d_c$ provided that the edge plasma is rotating sufficiently fast. It follows that in the presence of strong plasma rotation the kink mode stability boundaries are close to those calculated assuming that the vacuum vessel is a perfect conductor. If the vessel time-constant or the dissipation (i.e. S_* or ν_*, respectively) are sufficiently large then the stabilization criterion (85) reduces to

$$\Omega_0 > \sqrt{1 - d/d_c}. \tag{86}$$

In this limit the critical rotation rate just depends on the radius of the vacuum vessel and the critical radius for ideal instability. Note, from Eq. (67), that the simplified dispersion

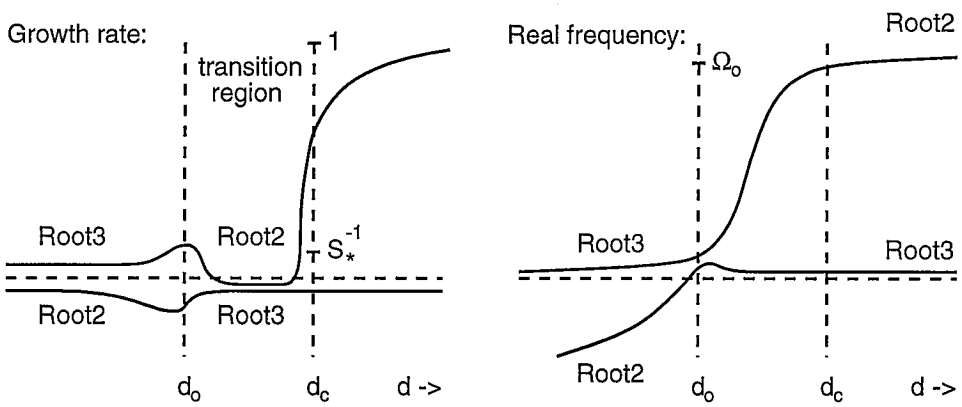

Figure 5: A schematic diagram showing the two non-trivial roots of the simplified dispersion relation (77) as functions of the vessel "spacing" d for non-zero normalized plasma rotation Ω_0. d_c is the critical vessel "spacing" for the stability of the ideal external-kink mode. d_0 is defined in Eq. (84). Note that the two roots cross over when $d = d_0$.

relation is only valid when $|g| \ll 1$. It follows from Eqs. (72) that the above stabilization criteria are only accurate when

$$Z \equiv \frac{(3c/d)\,(1 - d/d_c)}{(1 - c/d_c)^2} \ll 1, \tag{87}$$

which is most likely to be the case when the vessel radius lies just inside the critical radius for ideal instability (i.e. when d is just less than d_c).

2.7 An Inviscid Dispersion Relation

2.7.1 Derivation of the Dispersion Relation

In the inviscid limit

$$4 S_c \nu_c \ll g^2 \ll 1 \tag{88}$$

Eq. (42) yields

$$k_+^{\,2} \simeq \frac{g}{\nu_c}, \qquad k_-^{\,2} \simeq \frac{S_c}{g}, \tag{89}$$

implying that the width of the "skin current" layer is determined predominantly by plasma resistivity (since $|k_+| \gg |k_-|$). In this limit Eqs. (49) and (51) give

$$\overline{\psi}_+ + \overline{\psi}_- \simeq g^2 \sqrt{\frac{g}{S_c}}, \tag{90}$$

where the square root is taken such that the real part is positive. Finally, Eqs. (53), (54), and (70) yield

$$c\Delta_a \simeq (1 - c/d_c)^2 \left(\frac{g^2}{3} - g^2 \sqrt{\frac{g}{S_c}} \right). \tag{91}$$

By analogy with Section 2.6.1 the dispersion relation is written

$$\left((\widehat{\gamma} + \mathrm{i}\,\Omega_0)^2 - \sqrt{\eta_*}\,(\widehat{\gamma} + \mathrm{i}\,\Omega_0)^{5/2} + 1 - \frac{d}{d_c} \right) (S_* \widehat{\gamma} + 1 + md) \simeq 1 - (md)^2, \tag{92}$$

where

$$\eta_* = \frac{9}{c n s_a} \sqrt{\frac{3c}{d}} \frac{\tau_A}{c^2 \tau_R} \Big/ (1 - c/d_c). \tag{93}$$

This dispersion relation is similar to the previous dispersion (77) except that the dissipative term involving viscosity in the "skin current" layer is replaced by one involving resistivity. Normally, $\eta_* \ll 1$ because plasma resistive time-scales are typically long compared to Alfvénic time-scales.

2.7.2 The Roots of the Dispersion Relation

If the small dissipative term involving η_* is neglected then the above dispersion relation reduces to a simple cubic. The three roots are similar to those described in Section 2.6.2. The resistive corrections to each of these roots are easily calculated under the assumption that $\eta_* \ll 1$. If the vacuum vessel is sufficiently close to the plasma that the ideal external-kink mode is stabilized (i.e. if $d < d_c$), Root1 can be written

$$\widehat{\gamma} \simeq -\mathrm{i} \left(\Omega_0 + \sqrt{1 - d/d_c} \right) - \frac{1 - (md)^2}{2 S_* \sqrt{1 - d/d_c} \left(\Omega_0 + \sqrt{1 - d/d_c} \right)}$$

$$- \exp(-\mathrm{i}\,\pi/4)\,(1 - d/d_c)^{3/4}\,\frac{\sqrt{\eta_*}}{2}, \tag{94}$$

Root2 takes the form

$$\widehat{\gamma} \simeq -\mathrm{i}\left(\Omega_0 - \sqrt{1-d/d_c}\right) + \frac{1-(md)^2}{2S_*\sqrt{1-d/d_c}\left(\Omega_0 - \sqrt{1-d/d_c}\right)}$$

$$- \exp(+\mathrm{i}\,\pi/4)\,(1-d/d_c)^{3/4}\,\frac{\sqrt{\eta_*}}{2}, \tag{95}$$

and Root3 becomes

$$\widehat{\gamma} \simeq \exp(-\mathrm{i}\,\pi/4)\,{\Omega_0}^{5/2}\,\frac{\sqrt{\eta_*}\,(1-(md)^2)}{S_*(1-d/d_c-{\Omega_0}^2)^2}$$

$$+ \frac{(1-md_c)(1+md)\,d/d_c + (1+md)\,{\Omega_0}^2}{S_*(1-d/d_c-{\Omega_0}^2)}. \tag{96}$$

As before, Root1 is unconditionally stable. Root3, which corresponds to the resistive shell mode, is robustly unstable when $d < d_0$ (d_0 is defined in Eq. (84)) and robustly stable when $d > d_0$. Root2, which corresponds to the external-kink mode, is destabilized by the finite resistivity of the vacuum vessel and stabilized by resistive dissipation in the "skin current" layer. The resistive shell mode and the external-kink mode can be simultaneously stabilized by plasma rotation provided

$$\Omega_0 > \sqrt{1-d/d_c} + \frac{1-(md)^2}{S_*\sqrt{\eta_*/2}\,(1-d/d_c)^{5/4}}. \tag{97}$$

Note, again, that if the vessel time-constant or the dissipation (i.e. S_* or η_*, respectively) are sufficiently large then the stabilization criterion reduces to Eq. (86), which is independent of the dissipation.

2.8 Discussion

The amount of edge plasma rotation required to significantly alter the stability of a non-rotating helical kink mode, such as a resistive shell mode, is of order

$$\omega_0 \gtrsim (k_\parallel v_A)_a, \tag{98}$$

where $v_A \equiv R_0/\tau_A$ is the Alfvén velocity. It is easily demonstrated that

$$\frac{\omega_0}{(k_\parallel v_A)_a} \simeq \frac{\omega_0 \tau_A}{n s_a\, c} = \mathrm{Im}(g) \tag{99}$$

(see Eqs. (30f) and (31)). Clearly, stabilization is only likely when $\mathrm{Im}(g) \gtrsim O(1)$. Note that the critical rotation rate is significantly sub-Alfvénic (i.e. $\omega_0 \tau_A \ll 1$) since the parameter c is generally much less than unity. This ordering (which is equivalent to saying that an external-kink mode is only unstable when its associated mode rational surface lies just outside the edge of the current carrying plasma) comes about naturally because external-kink eigenfunctions are peaked in the outer regions of the plasma, so if $c \ll 1$ then $(k_\parallel R_0)_a \simeq n s_a\, c \ll 1$ and the stabilizing influence of magnetic field-line bending is minimized [24].

According to the simplified dispersion relations (77) and (92), stabilization of the resistive shell mode is due to the combined effects of plasma inertia and dissipation. Above a certain critical rotation rate, plasma inertia acting in the relatively thick inertial layer converts the essentially non-rotating, robustly unstable resistive shell mode root of the dispersion relation (Root 3) into a rotating, almost marginally stable kink mode root (Root 2). The latter root is slightly destabilized by the resistivity of the vacuum vessel but is stabilized by plasma dissipation (either viscous or resistive) acting in the relatively thin "skin current" layer. Thus, given sufficient plasma rotation and dissipation, all of the roots of the external-kink dispersion relation are stable (assuming, of course, that the vacuum vessel is sufficiently close to the plasma to stabilize the *ideal* external-kink mode).

In the presence of strong dissipation the critical rotation rate required to stabilize the resistive shell mode reduces to

$$\frac{\omega_0}{(k_\parallel v_A)_a} \simeq \frac{\omega_0 \tau_A}{n s_a\, c} \geq \sqrt{\frac{3c}{d}}\frac{\sqrt{1-d/d_c}}{(1-c/d_c)} \tag{100}$$

(see Eqs. (72b) and (86)), which is independent of the dissipation. Note from Eqs. (77) and (92) that plasma rotation modifies the external-kink dispersion relation principally via the

contribution from the relatively wide inertial layer. Thus, the above critical rotation rate is to be understood as a critical rotation rate of the plasma located within a radial distance $c\,a$ (i.e. about the same as the distance of the rational surface from the edge of the plasma) from the edge of the current carrying plasma.

Equation (100) indicates that the critical rotation rate is a strongly increasing function of c; i.e. the distance of the rational surface from the plasma. External-kink modes tend to become more stable as $c \propto (R_0 k_\parallel)_a$ increases, so, rather paradoxically, strongly unstable resistive shell modes are easier to stabilize (i.e. they require less plasma rotation) than weakly unstable modes. According to Eq. (100), the critical rotation rate for close-fitting vacuum vessels exceeds that for loose-fitting vessels. This is also somewhat counter-intuitive. The basic form of the dispersion relation, Eq. (66), describes the coupling of the currents flowing in the edge region of the plasma (comprising the inertial and "skin current" layers) to those flowing in the vacuum vessel. The strength of the coupling scales like $1/d$; i.e. it becomes stronger as the vacuum vessel moves closer to the edge of the plasma. The stabilization of the resistive shell mode comes about because plasma rotation decouples the edge from the vacuum vessel. Clearly, the level of rotation required to achieve this increases with the coupling strength. The optimum configuration is to minimize the coupling by placing the vacuum vessel as far away from the plasma as possible; i.e. just inside the critical radius for stabilizing the ideal external-kink mode. Indeed, it can be seen from Eq. (100) that the critical rotation rate becomes very small as $d \rightarrow d_c$.

Equations (74), (76), and (85) indicate that viscous dissipation is sufficiently strong that it drops out of the stabilization criterion provided

$$\tau_{\rm w} \gg \frac{5}{12}\frac{1-(md)^2}{1-d/d_c}\frac{c^2\tau_V}{d}. \tag{101}$$

A similar, but more complicated, inequality (involving the resistive time-scale τ_R, instead of the viscous time-scale τ_V) is obtained from Eq. (97) in the resistive regime. Clearly, the

"dissipationless" critical rotation rate (100) is valid provided that the L/R time of the vacuum vessel is sufficiently long. For "leaky," short time-constant vacuum vessels plasma dissipation can significantly increase the critical rotation rate. Plasma dissipation is also more likely to be a problem close to the ideal stability boundary when $d \rightarrow d_c$ (see Eq. (101)).

3 NUMERICAL RESULTS

The "Computational Toroidal Device" (CTD) code is a toroidal, spectral, initial-value, implicit, single-fluid, linear, MHD stability code which includes compressibility and handles sheared plasma rotation in a self-consistent manner [25]. In order to check the analytic dispersion relation derived above, the CTD code has been used to simulate a cylindrical plasma with uniform toroidal rotation. In these simulations the density and perpendicular viscosity are uniform throughout the plasma; i.e. from the magnetic axis to the radius of the vacuum vessel, $r = r_{\rm w}$. Free-slip boundary conditions (i.e. $v_r = 0$ and $v_\theta' = 0$) are applied at the outer radius of the plasma. These conditions are consistent with no-slip boundary conditions (i.e. $v_r = 0$ and $v_\theta = 0$), assuming the existence of an unresolved viscous boundary layer just inside the vacuum vessel. The plasma resistivity is uniform between the magnetic axis and the outer radius of the hot, current carrying plasma, $r = a$. In the region between $r = a$ and $r = r_{\rm w}$ the plasma resistivity is extremely high ($\eta = 10^4$ in normalized units where all lengths are scaled to the minor radius of the hot plasma, a, and all times to the Alfvén time, τ_A). Thus, the region between the edge of the hot plasma and the vacuum vessel acts like a cold dense plasma (i.e. it is far too resistive to carry any significant current, but possesses non-negligible inertia and viscosity). The vacuum vessel itself is treated as a rigid annular region of low resistivity (relative to the cold plasma). The region outside the vacuum vessel, $r > r_{\rm w}$, acts like a true vacuum (i.e. the resistivity is large, $\eta = 10^4$, and there is no fluid, $\mathbf{v} = \mathbf{0}$). This vacuum region extends out to twice the radius of the hot plasma, $r = 2a$, at which point the simulation is truncated by the presence of a perfectly conducting shell.

The CTD simulation differs from the analytic model in three respects. Firstly, it allows compressible motion of the plasma; secondly, the cold plasma in the region $a < r < r_{\rm w}$ possesses non-negligible inertia and viscosity; and, finally, there is a perfectly conducting shell at $r = 2a$. The plasma flow is expected to be almost incompressible in this particular problem, since $|\gamma_0| \gg |k_\parallel c_s|$ throughout most of the plasma (especially close to the edge where most of the important physics takes place). In fact, results from CTD show quite clearly that the compressible component of the plasma motion is always far smaller than the incompressible component. Special test runs of CTD in which the inertia and viscosity of the cold plasma region are gradually taken to zero demonstrate that the presence of inertia and viscosity in this region has very little effect (i.e. $\lesssim 10\%$) on kink mode growth-rates. It is easily shown (and can also be explicitly verified using CTD) that a perfectly conducting shell at $r = 2a$ is sufficiently far from the plasma that it also has very little influence (i.e. $\lesssim 10\%$) on kink mode growth-rates. Clearly, the differences between the CTD simulations and the analytic model are relatively unimportant, so both ought to give similar results.

The current profile used in the simulations is the well-known "Wesson profile" [24]

$$j_z(r) = j_z(0)\left(1 - \frac{r^2}{a^2}\right)^{q_a/q_0 - 1}, \tag{102}$$

where $q_0 \equiv q(0)$ is the central safety-factor of the plasma and $q_a \equiv q(a)$ is the edge value. The Wesson profile has the advantage that the current is zero at the edge of the hot plasma provided $q_a > 2q_0$ (which is always the case in the simulations presented here). Note, from Eq. (25), that a non-zero current at the plasma edge modifies the matching conditions there and, thereby, changes the kink mode stability boundaries (usually in a detrimental manner). The above current profile can be inverted to give the safety-factor profile:

$$q(r) = q_a \frac{r^2/a^2}{1 - (1 - r^2/a^2)^{q_a/q_0}} \tag{103}$$

(see Eq. (7)). This profile can be used, in conjunction with the marginally-stable ideal-MHD equations (26), to fix the parameter d_c (defined in Eq. (28)). This parameter is related to

the critical vacuum vessel radius, r_c, required to stabilize the *ideal* external-kink mode, via Eq. (83). Table 1 shows various values of d_c and r_c evaluated numerically from Eqs. (26) and (103) for the $m = 2/n = 1$ external-kink mode. There is almost perfect agreement between the critical vessel radius evaluated in this manner and that inferred from the CTD code.

q_a	d_c	r_c/a
1.6	0.3461	1.531
1.7	0.2919	1.397
1.8	0.2375	1.295
1.9	0.1812	1.209
1.99	0.1186	1.128

Table 1: Values of d_c and the critical vessel radius r_c required to stabilize the 2/1 ideal external-kink mode calculated as functions of the edge safety-factor q_a using a Wesson-like current profile with central safety-factor $q_0 = 0.8$

Figure 6(a) shows the 2/1 ideal external-kink mode growth-rate evaluated at zero plasma rotation as a function of the vessel radius using both the analytic model (i.e. Eqs. (42), (49), (51), (53), (54), (56), (61), and (66)) and the CTD code. In this comparison $q_0 = 0.8$, $q_a = 1.8$, the vessel resistivity is effectively zero, and the plasma resistivity and viscosity are negligible. The analytic growth-rates are slightly higher than the numerical ones but, otherwise, there is very good agreement between the two. This indicates that the central premise of Section 2 is correct; i.e. external-kink modes can be analyzed by splitting the hot current carrying plasma into a central ideal region surrounded by a relatively thin non-resonant inertial layer. It can be seen that both the analytic and numerical ideal growth-rates tend to zero as the vessel radius approaches the critical radius $r_c = 1.295$ (see Table 1). It is evident that the ideal mode is stable for $r_{\rm w} < r_c$.

Figure 6(a) also shows the zero rotation resistive shell mode growth-rates calculated for $r_{\rm w} < r_c$. In this comparison the current profile is the same as that used to calculate the ideal growth-rates. The time-constant of the vacuum vessel is $\tau_{\rm w} = 4000\, r_{\rm w}$ in normalized units (from now on all quantities are in normalized units unless explicitly stated otherwise).

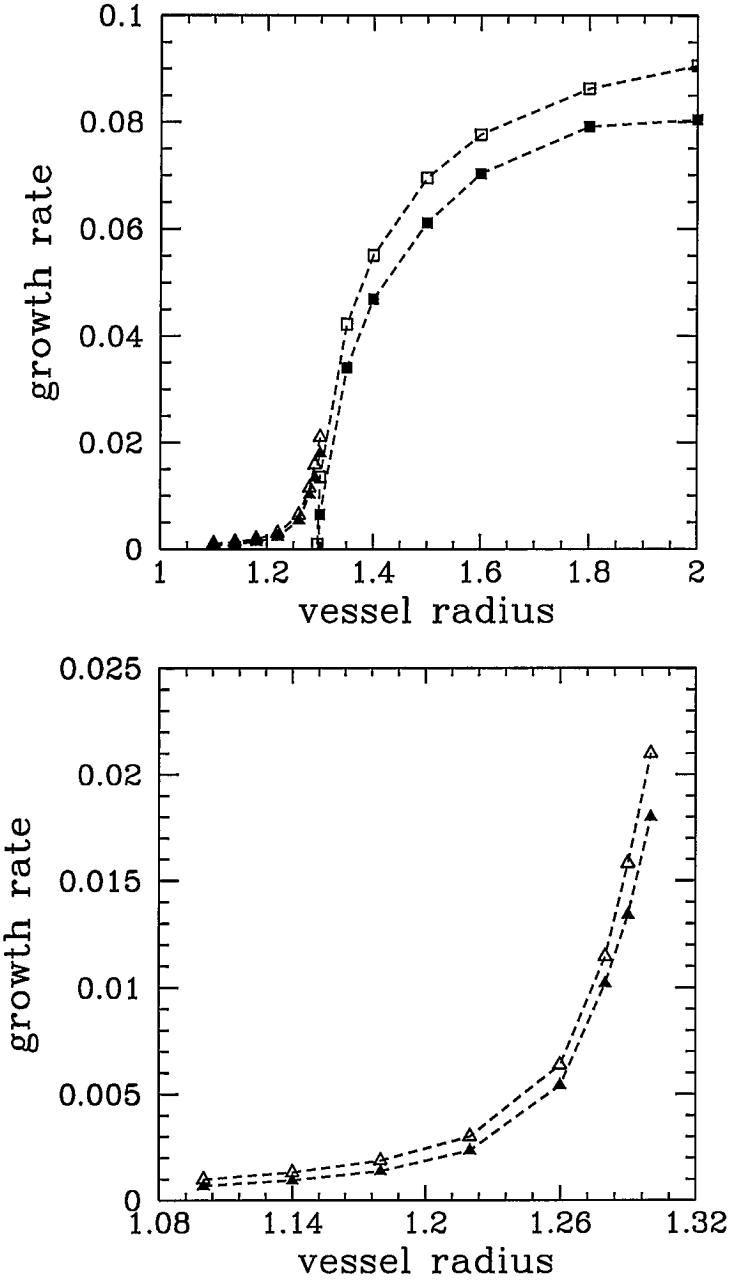

Figure 6: The growth-rate (normalized to the Alfvén time) of the 2/1 external-kink mode as a function of the vessel radius (normalized to the minor radius of the plasma). The solid symbols are numerical results from the CTD code. The open symbols are the predictions of the analytic dispersion relation. The square symbols are ideal external-kink growth-rates. The triangular symbols are resistive shell mode growth-rates.

The thickness of the vessel is 0.02 in the CTD simulations. This is sufficiently thin for the "thin shell" approximation used in the analytic model to be valid (see Section 2.5.2). The plasma resistivity and kinematic viscosity ($\nu \equiv \mu_\perp/\rho$) are both 10^{-5}. It can be seen that there is good agreement between the analytic and numerical growth-rates. The resistive and ideal growth-rates connect together smoothly as the vessel radius moves outside the critical radius. There is clearly no vessel radius at which either a resistive shell mode or an ideal external-kink mode is not unstable. Figure 6(b) is a blow-up of Fig. 6(a) showing the resistive shell mode growth-rates in more detail. The analytic growth-rates are slightly higher than the numerical ones. This discrepancy is small in absolute terms but becomes quite large in relative terms for slowly growing modes. The most likely reason for the discrepancy is the failure of asymptotic matching. This is only completely accurate when the widths of the non-ideal regions are completely negligible, which, of course, is never the case in the CTD simulations.

Figure 7(a) shows the growth-rate of the 2/1 resistive shell mode calculated as a function of plasma rotation for various vacuum vessel radii. The plasma and vessel parameters (with the exception of the plasma rotation) are the same as those used in Fig. 6(b). There is fairly good agreement between the numerical and analytic results. All of the features displayed by the CTD results are reproduced by the analytic model. A vacuum vessel which is far from the plasma gives rise to a resistive shell mode with a large zero frequency growth-rate. However, this mode is stabilized at relatively low plasma rotation rates. Conversely, a vacuum vessel which is close to the plasma yields a resistive shell mode with a small zero frequency growth-rate. However, this mode is only stabilized at relatively high plasma rotation rates. Thus, somewhat paradoxically, the optimum configuration in the absence of plasma rotation (i.e. a close-fitting vacuum vessel) is the worst configuration in the presence of strong rotation. In the latter case, the optimum configuration is for the vacuum vessel to be as far away from the plasma as is consistent with the stability of the ideal external-kink mode (see Section 2.8).

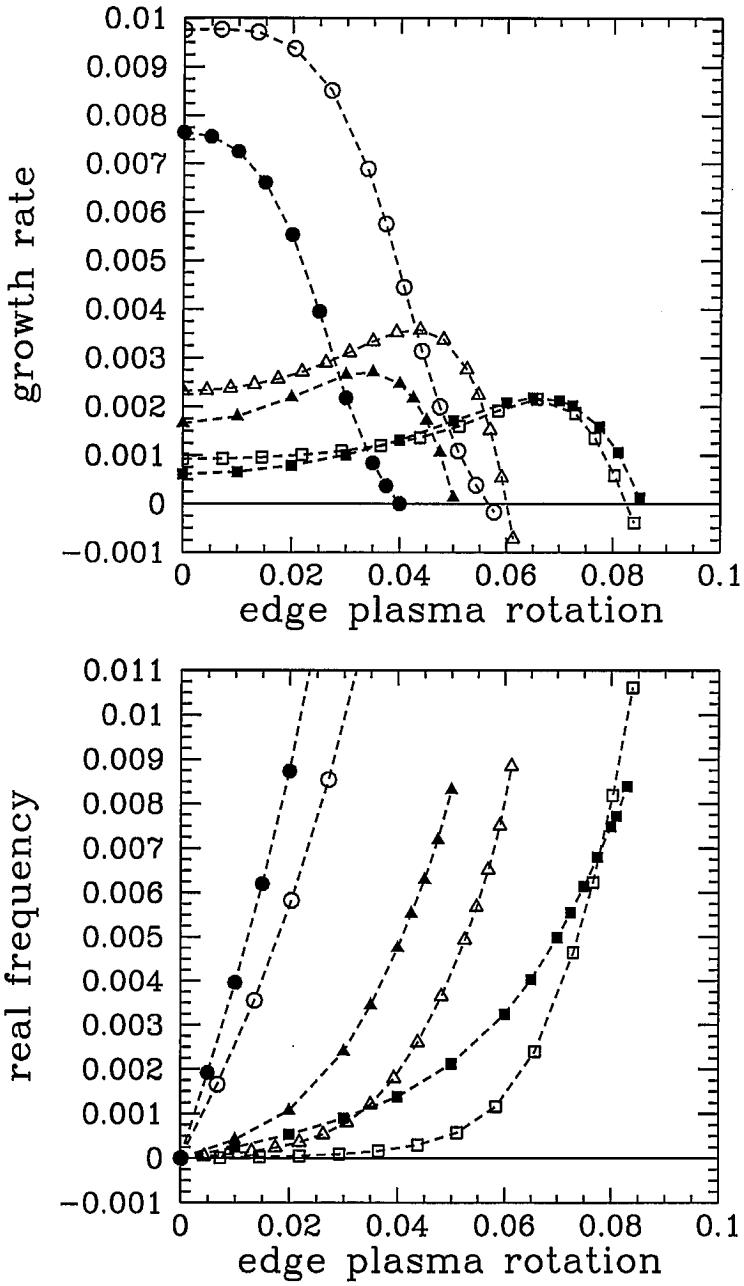

Figure 7: The growth-rate and real frequency of the 2/1 resistive shell mode as functions of plasma rotation and the vacuum vessel radius. The solid symbols are numerical results and open symbols are the corresponding analytic predictions. The round, triangular, and square symbols correspond to vacuum vessel radii of 1.275, 1.2, and 1.09, respectively.

Figure 7(b) shows the real frequency of the 2/1 resistive shell mode calculated as a function of plasma rotation for the three cases featured in Fig. 7(a). It can be seen that stabilization of the shell mode always takes place just as the magnitude of its real frequency starts to exceed its growth-rate. This is clearly a necessary condition for stabilization. However, it is not a sufficient condition, as can be seen from Eq. (81) where at low dissipation it possible to find strongly rotating solutions which are nevertheless unstable. Thus, it is the dissipation which is responsible for the stabilization of the shell mode. The acquisition of a substantial real frequency by the mode is incidental to the stabilization mechanism.

Table 2 lists some parameters of the analytic model for the three cases featured in Fig. 7. Also shown is the simplified estimate (85) for the critical plasma rotation rate required to stabilize the resistive shell mode. It can be seen, by comparison with Fig. 7(a), that this estimate is quite accurate when the vacuum vessel is far from the plasma, but is otherwise far too large. The simplified estimate is only valid when $Z \ll 1$ (see Eq. (87)), which is clearly not the case in those situations where it fails badly. In fact, the cubic dispersion relation (77), although useful for pedagogical purposes, does not give particularly good agreement with the CTD code. It generally seriously overestimates the critical rotation rate at which complete stabilization occurs. It also wildly exaggerates the slight tendency, apparent in Fig. 7(a), for the growth-rate to initially rise with increasing rotation. According to the full analytic dispersion relation (which agrees quite well with the CTD code) the simplified dispersion relation (77) is only applicable at relatively low rotation rates. As the edge plasma rotation increases plasma resistivity gradually takes over from viscosity as the principal dissipation mechanism. Also, inertial corrections (such as the g^2 terms in Eqs. (49), (51), (70), etc.) become increasingly important as the rotation rate gets larger. Inertial corrections are particularly significant for close-fitting vacuum vessels. Good agreement between the analytic model and the CTD code is only possible when viscous, resistive, and inertial effects are all simultaneously retained in the model.

$r_{\rm w}$	1.09	1.2	1.275
d	0.08533	0.1746	0.2255
d_c	0.2377	0.2377	0.2377
c	0.05556	0.05556	0.05556
ν_*	0.03837	0.05490	0.06237
S_*	75.40	118.7	143.4
Z	2.135	0.4316	0.06461
$(\omega_0\tau_A)_{\rm crit}$	0.2471	0.1100	0.07728

Table 2: Various parameters associated with the analytic model, evaluated for the three cases featured in Fig. 7. The final row shows the estimate (85) for the critical plasma rotation rate required to stabilize the resistive shell mode.

Figure 8 shows perturbed "toroidal" current eigenfunctions calculated by the CTD code for three different plasma rotation rates. The mode amplitudes and phases inside the plasma are identical in all three cases. The plasma and vessel parameters are the same as those employed in the case featured in Fig. 7 with $r_{\rm w} = 1.09$. It can be seen that the perturbed current is concentrated in the outer nonideal regions of the plasma, in accordance with the analysis of Section 2. The width of the nonideal region is about 0.05, which is in good agreement with the theoretically expected width c (note, from Table 2, that $c = 0.05556$ for these calculations). A (positive) "skin current" spike is also clearly visible, superimposed on a broader (negative) inertial layer current distribution. The spike gets bigger as the plasma rotation rate increases. This is as expected if the "skin current" spike is ultimately responsible for the stabilization of the resistive shell mode.

Figure 9 shows the growth-rate of the 2/1 resistive shell mode calculated as a function of plasma rotation for various vacuum vessel time-constants. In these calculations the plasma resistivity and kinematic viscosity are both 10^{-5}. The other parameters are $q_0 = 0.8$, $q_a = 1.8$, $r_c = 1.295$, and $r_{\rm w} = 1.09$. It can be seen that, in general agreement with Eqs. (85), (97), and (101), long time-constant vessels perform significantly better (in terms of the level of plasma rotation required to stabilize the shell mode) than short time-constant vessels. This particular trend is slightly more marked in the numerical results.

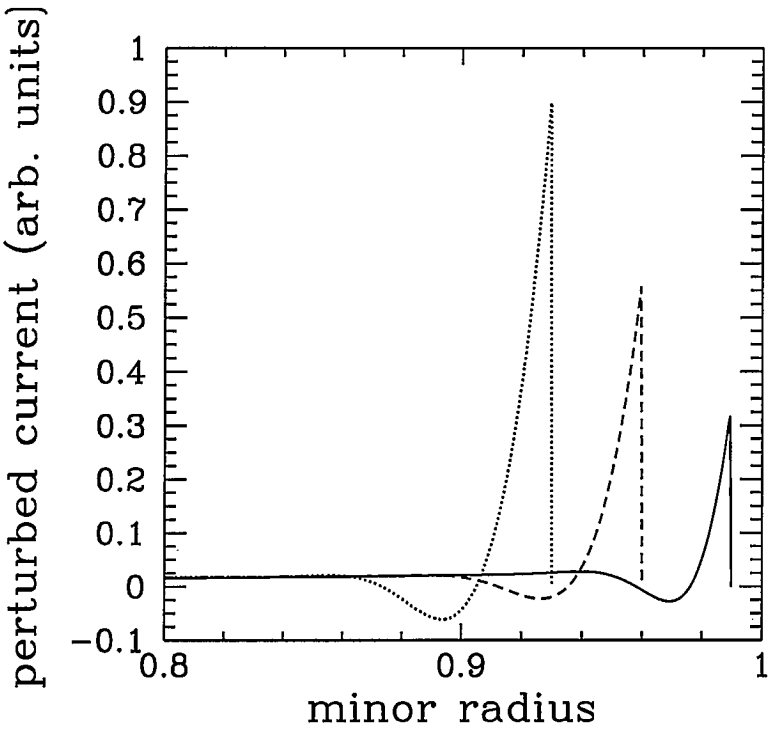

Figure 8: The perturbed "toroidal" current eigenfunction (for fixed mode amplitude and phase inside the plasma) in the outer regions of the plasma calculated by the CTD code for the case with $r_w = 1.09$ featured in Fig. 7. The solid, dashed, and dotted lines correspond to plasma rotations of 0.01, 0.06, and 0.08, respectively. For the sake of clarity the curves are offset horizontally. In reality, the sudden cut-off in the current occurs at $r = 1$ in all three cases.

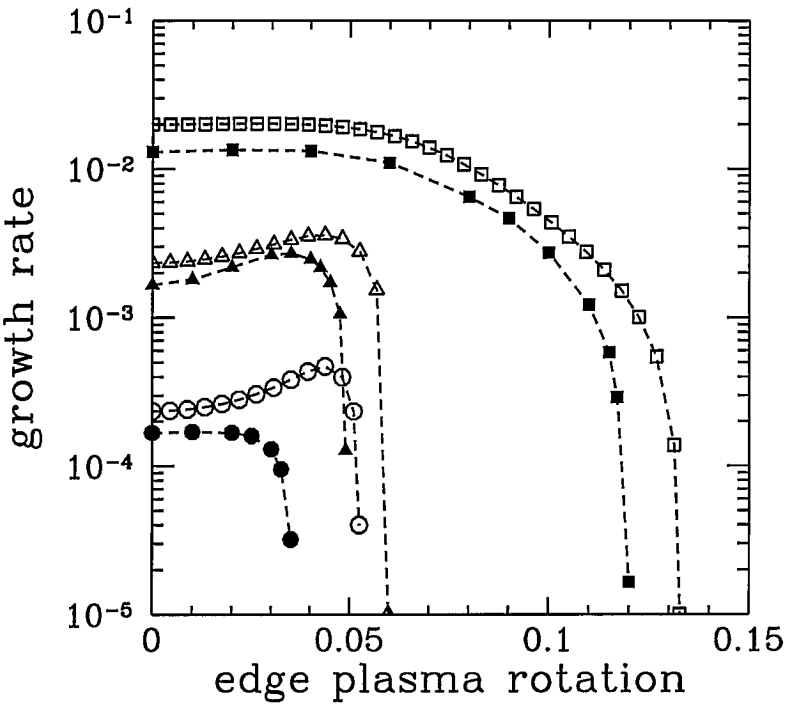

Figure 9: The growth-rate of the 2/1 resistive shell mode as a function of plasma rotation and the vessel time-constant. The solid symbols are numerical results and open symbols are the corresponding analytic predictions. The round, triangular, and square symbols correspond to time-constants of $40000\,r_{\rm w}$, $4000\,r_{\rm w}$, and $400\,r_{\rm w}$, respectively.

4 FINITE THICKNESS VACUUM VESSELS

The "thin shell" dispersion relation (61) is only valid when the inequality (63) is satisfied. The more general expression

$$\Delta_{\rm w} = \sqrt{\gamma\tau_{\rm w}\, r_{\rm w}/\delta_{\rm w}}\,\tanh\left(\sqrt{\gamma\tau_{\rm w}\,\delta_{\rm w}/r_{\rm w}}\right) \tag{104}$$

is valid provided

$$|\gamma|\tau_{\rm w} \gg \frac{\delta_{\rm w}}{r_{\rm w}}. \tag{105}$$

For relatively thin vacuum vessels, where $|\gamma|\tau_{\rm w} \ll r_{\rm w}/\delta_{\rm w}$, the above dispersion relation reduces to the "thin shell" limit. On the other hand, for relatively thick vacuum vessels,

where $|\gamma|\tau_w \gg r_w/\delta_w$, the dispersion relation gives the "thick shell" limit

$$\Delta_w = \sqrt{\gamma \tau_w \, r_w/\delta_w}. \tag{106}$$

Figure 10 shows the growth-rate of the 2/1 resistive shell mode calculated as a function of plasma rotation for vacuum vessels of various thicknesses, but the same overall time-constant. The analytic calculations are performed using Eq. (104) instead of Eq. (61) in the external-kink dispersion relation (66). The plasma and vessel parameters (other than the vessel thickness) are the same as those employed in the case featured in Fig. 7 with $r_w = 1.2$. It can be seen that a thick vacuum vessel does not perform as well as a thin vessel possessing the same time-constant. The zero-rotation growth-rate and the critical rotation rate required to stabilize the shell mode are both significantly increased in the former case. This suggests that it is better to surround the plasma with a thin vessel made of a highly conducting material rather than a thicker vessel made of a more resistive material.

5 INCOMPLETE STABILIZING SHELLS

In many modern tokamak designs the vacuum vessel is too remote from the plasma to significantly affect kink stability. However, such designs often incorporate additional passive conductors to guard against external-kink modes. These conductors are usually placed very close to the plasma ($r_w \sim 1.05$, say) but are necessarily *highly incomplete* due to space and access requirements. Consider the rather idealized case of a plasma surrounded by a concentric passive stabilizing shell of uniform thickness but containing toroidal gaps (i.e. gaps extending over a range of toroidal angles). In the "thin shell" regime the dispersion relation of the shell (i.e. the replacement to Eq. (61) in the full dispersion relation (66)) is written [26]

$$\Delta_w = \frac{\gamma \tau_w (1-f)}{1 + \gamma \tau_w f/2m}, \tag{107}$$

where f is the angular fraction of the gaps (the distribution of gaps does not matter, as long as they are sufficiently large) and τ_w is the time-constant of the shell with no gaps ($f = 0$).

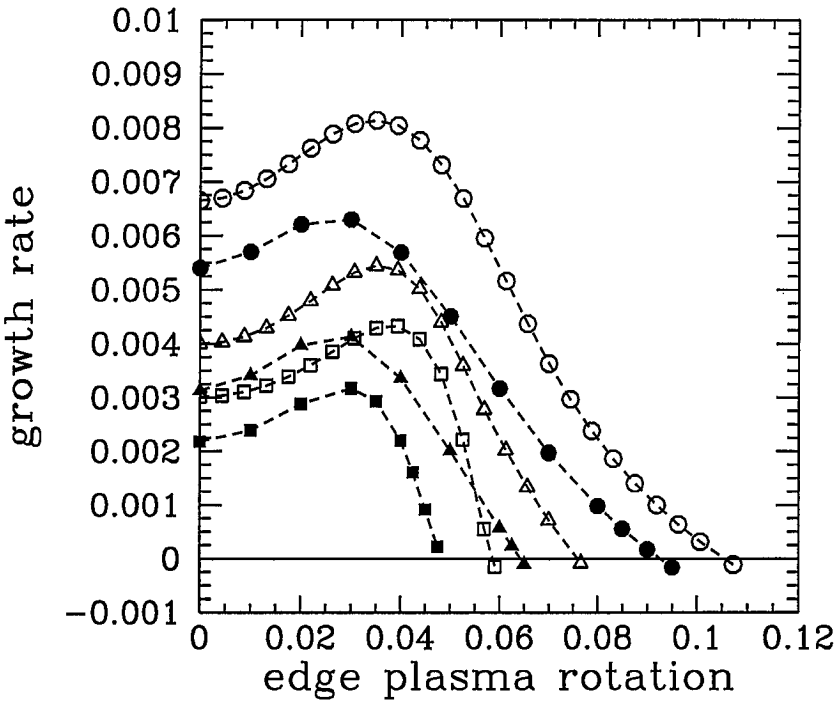

Figure 10: The growth-rate of the 2/1 resistive shell mode as a function of plasma rotation and the vessel thickness. The solid symbols are numerical results and open symbols are the corresponding analytic predictions. The round, triangular, and square ymbols correspond to vessel thicknesses of 0.32, 0.16, and 0.08, respectively.

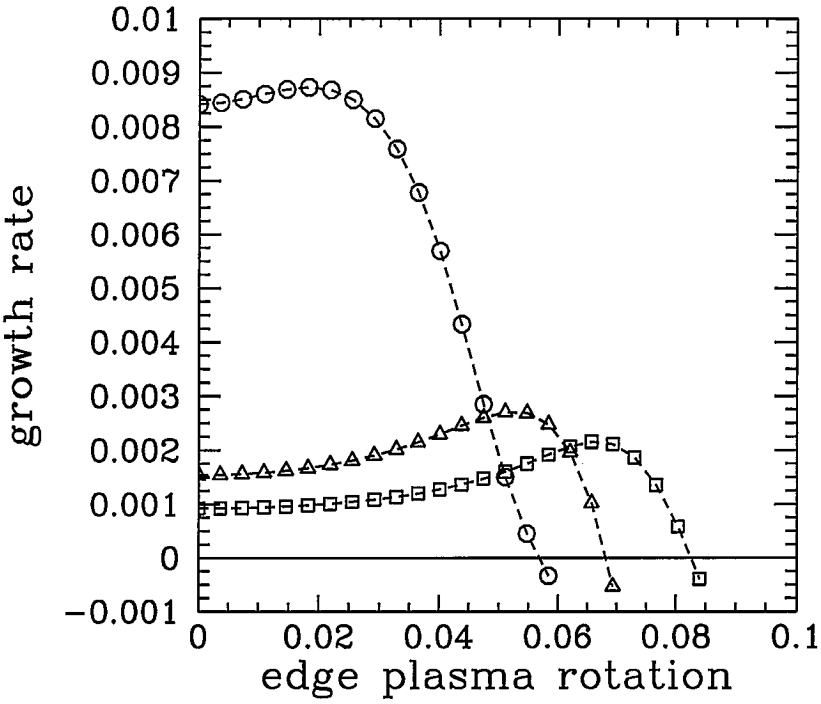

Figure 11: The growth-rate of the 2/1 resistive shell mode as a function of plasma rotation and the toroidal gap size. The results shown are all analytic predictions. The round, triangular, and square symbols correspond to toroidal gaps of angular (fractional) extent 162° (0.45), 72° (0.2), and 0° (0), respectively.

Figure 11 shows the growth-rate of the 2/1 resistive shell mode calculated as a function of plasma rotation for a close-fitting ($r_{\rm w} = 1.09$) stabilizing shell containing toroidal gaps of various sizes. The plasma parameters are the same as those employed in the cases featured in Fig. 7. The time-constant of the shell in the absence of gaps is $\tau_{\rm w} = 4000\, r_{\rm w}$. It can be seen, by comparison with Fig. 7(a), that a close-fitting stabilizing shell containing gaps acts very much like a complete shell located somewhat further away from the plasma. This is a significant result. For a complete close-fitting shell the level of plasma rotation required to stabilize the resistive shell mode can be prohibitively high. However, a stabilizing shell does not have to be complete (unlike a vacuum vessel). By a judicious choice of gap size the required level of plasma rotation can be significantly reduced. This effect becomes increasingly marked as the spacing between the shell and the plasma is reduced. Of course, if the gaps are made too large then the effective radius of the shell will move outside the critical radius for stabilizing the ideal external-kink mode. At this point, the mode "explodes" though the gaps with an ideal growth rate [26]. In Fig. 11 the case with 162° of gaps is very close to the ideal stability boundary.

6 THE EFFECT OF SIDEBAND RESONANCES

It is necessary to adopt a slightly more flexible notation in order to deal with coupled sideband rational surfaces inside the plasma. The cylindrical dispersion relation (66) can be written in standard E-Matrix format [27] as

$$\left(\begin{array}{cc} \Delta_a - E_{aa} & -E_{a\rm w} \\ -E_{a\rm w} & \Delta_{\rm w} - E_{\rm ww} \end{array} \right) \left(\begin{array}{c} \Psi_a \\ \Psi_{\rm w} \end{array} \right) = \left(\begin{array}{c} 0 \\ 0 \end{array} \right). \tag{108}$$

This dispersion relation is reminiscent of that of two coupled tearing modes. However, in this case there are no tearing layers in the plasma. The nonideal regions (which are radially localized, like conventional tearing layers) occur at the plasma edge (labeled by the subscript $_a$) and at the vacuum vessel (labeled by the subscript $_{\rm w}$). The outer ideal solution is described

by two complex parameters: the m/n perturbed poloidal flux at the edge of the plasma, Ψ_a, and the perturbed flux at the vessel radius, $\Psi_{\rm w}$. The non-ideal layers are characterized by two complex parameters: the jump in logarithmic derivative of the m/n perturbed poloidal flux across the edge layer, Δ_a, and the jump in logarithmic derivative across the vacuum vessel, $\Delta_{\rm w}$. These layer parameters depend on the complex growth-rate of the mode, the edge plasma rotation, and the L/R time of the vessel. Finally, asymptotic matching between the outer solution and the layer solutions is achieved via the elements of the E-Matrix (E_{aa}, etc). These are $O(1)$ real parameters which depend only on the properties of the outer eigenfunctions. It can be demonstrated that

$$\begin{aligned} E_{aa} &= \frac{1}{d_c} - \frac{1}{d}, \\ E_{a{\rm w}} &= \frac{\sqrt{1-(md)^2}}{d}, \\ E_{\rm ww} &= -\frac{1+md}{d}. \end{aligned} \tag{109}$$

The above dispersion relation can easily be generalized to take into account the presence of a toroidally coupled $(m-1)/n$ sideband rational surface located somewhere inside the plasma at radius $r_s < a$. In order to describe the outer solution an additional complex parameter is required: the $(m-1)/n$ perturbed poloidal flux at the rational surface, Ψ_s, which is usually referred to as the "reconnected flux." An additional complex layer parameter is also needed: the jump in logarithmic derivative of the $(m-1)/n$ perturbed poloidal flux across the rational surface, Δ_s. Asymptotic matching between the outer solution and the layer solutions yields a dispersion relation of the form

$$\begin{pmatrix} \Delta_a - E_{aa} & -E_{a{\rm w}} & -E_{as} \\ -E_{a{\rm w}} & \Delta_{\rm w} - E_{\rm ww} & -E_{s{\rm w}} \\ -E_{as} & -E_{s{\rm w}} & \Delta_s - E_{ss} \end{pmatrix} \begin{pmatrix} \Psi_a \\ \Psi_{\rm w} \\ \Psi_s \end{pmatrix} = \begin{pmatrix} 0 \\ 0 \\ 0 \end{pmatrix}. \tag{110}$$

The $O(1)$ parameter E_{ss} governs the stability of the $(m-1)/n$ fixed-boundary tearing mode. This mode is assumed to be stable, for the sake of simplicity, so $E_{ss} < 0$. The parameters

E_{as} and E_{sw} describe coupling between neighboring poloidal harmonics and are, therefore, of order ϵ (where $\epsilon \ll 1$ is the inverse aspect ratio). The effects of any coupled harmonics other than m/n and $(m-1)/n$ are neglected in Eq. (110). In addition, the vacuum vessel is assumed to act as a perfect conductor as far as the $(m-1)/n$ harmonic is concerned. These rather drastic approximations are made to elucidate the analysis.

Adopting the normalization of Section 2.6, plus the rather restrictive ordering (67), the dispersion relation of the edge layer becomes (see Eq. (73))

$$d\,\Delta_a \simeq (\widehat{\gamma} + \mathrm{i}\,\Omega_0)^2 + \nu_*(\widehat{\gamma} + \mathrm{i}\,\Omega_0). \tag{111}$$

In the "thin shell" limit the dispersion relation of the vacuum vessel reduces to (see Eq. (75))

$$d\,\Delta_{\rm w} = S_*\,\widehat{\gamma}. \tag{112}$$

Finally, in a strongly rotating plasma the appropriate dispersion relation for the sideband rational surface is [28]

$$\Delta_s \simeq -\frac{S_s}{\widehat{\gamma} + \mathrm{i}\,\Omega_s}. \tag{113}$$

Here,

$$\begin{aligned} S_s &= \sqrt{\frac{d}{3c}}\,(1 - c/d_c)\,\frac{s_s}{s_a}\frac{\tau_A}{\tau_{As}}\frac{\pi}{c}, \\ \Omega_s &= \sqrt{\frac{d}{3c}}\,(1 - c/d_c)\,\omega_s\tau_A \Big/ (c\,n s_a), \end{aligned} \tag{114}$$

where $s_s = (\ln q/d\ln r)_{r_s}$ is the magnetic shear and $\tau_{As} = R_0\sqrt{\mu_0\rho(r_s)}/B_z$ the hydromagnetic time-scale at the rational surface, and ω_s is the natural frequency of the $(m-1)/n$ tearing mode. Note that $\omega_s = (m-1)\,\Omega_{\theta\,s} - n\,\Omega_{z\,s}$, where $\Omega_{\theta\,s}$ and $\Omega_{z\,s}$ are, respectively, the poloidal and "toroidal" plasma angular rotation velocities at the rational surface. The dispersion relation (113) describes dissipation via absorption of Alfvén waves at the resonant layer.

The (nearly) non-rotating root (Root3 in the terminology of Section 2.6.2) of the dispersion relation (110) can be shown to take the form

$$\widehat{\gamma} \simeq -\mathrm{i}\,\Omega_0\,\frac{\nu_*(1-(md)^2)}{S_*(1-d/d_c-{\Omega_0}^2)^2}+\frac{(1-md_c)(1+md)\,d/d_c+(1+md)\,{\Omega_0}^2}{S_*(1-d/d_c-{\Omega_0}^2)}$$

$$-\mathrm{i}\,\frac{\zeta_s\Omega_s}{S_*}\left\{1+\frac{(E_{as}/E_{sw})\sqrt{1-(md)^2}}{(1-d/d_c-{\Omega_0}^2)}\right\}, \tag{115}$$

where

$$\zeta_s=\frac{d\,(E_{sw})^2}{S_s}\ll 1 \tag{116}$$

In deriving Eq. (115) it is assumed that $S_* \gg 1$, $\nu_* \ll 1$, and $S_s \gg 1$. It can be seen, by comparison with Eq. (82), that the sideband resonance gives rise to an additional (small) contribution to the real frequency of Root3 but does not affect its growth-rate. For sufficiently strong edge plasma rotation (i.e. $\Omega_0 > \sqrt{1-d/d_c}$) the root is stable.

The rotating root (Root2 in the terminology of Section 2.6.2) of the dispersion relation (110) can be shown to take the form

$$\widehat{\gamma} \simeq -\mathrm{i}\left(\Omega_0-\sqrt{1-d/d_c}\right)+\frac{1-(md)^2}{2S_*\sqrt{1-d/d_c}\left(\Omega_0-\sqrt{1-d/d_c}\right)}-\frac{\nu_*}{2}$$

$$-\frac{\zeta_s}{2}-\frac{\zeta_s(\Omega_s-\Omega_0)}{2\sqrt{1-d/d_c}}. \tag{117}$$

It can be seen, by comparison with Eq. (81), that the sideband resonance gives rise to two additional terms. The first, $\zeta_s/2$, is stabilizing and is similar in form to the term $\nu_*/2$ which describes viscous dissipation in the edge layer. Recall that the edge dissipation is vital to the stabilization of the rotating root in the regime where the edge plasma rotation is sufficiently strong to stabilize the non-rotating root. It is clear that the Alfvénic dissipation at the sideband rational surface has an equivalent stabilizing effect. Thus, the combination of strong edge plasma rotation and dissipation *anywhere in the plasma* is capable of stabilizing the resistive shell mode. The second additional term in Eq. (117) is proportional to the

rotation shear, $\Omega_s - \Omega_0$, between the plasma at the sideband rational surface and the edge plasma. If this shear is positive (i.e. the central plasma rotates faster than the edge plasma) then the dissipation at the sideband rational surface is enhanced. However, if the shear is negative (i.e. the central plasma rotates slower than the edge plasma) then the dissipation is reduced. Clearly, for fixed levels of edge rotation it is better to have the center of the plasma rotating faster than the edge.

7 CONCLUSIONS

Stabilization of the resistive shell mode in toroidal pinch devices is possible provided that three conditions are met. First, the edge rotation $\omega_0 = m\,\Omega_\theta - n\,\Omega_\phi$ (where Ω_θ and Ω_ϕ are, respectively, the poloidal and toroidal angular rotation velocities of the edge plasma) must exceed a critical value:

$$\omega_0 \tau_A \geq (\omega_0 \tau_A)_{\rm crit} \simeq (k_\parallel R_0)_a. \tag{118}$$

Here, $(k_\parallel)_a$ is the parallel wavenumber of the instability and τ_A is the Alfvén time-scale; both are evaluated at the boundary of the current carrying plasma. Second, there must be a small amount of dissipation somewhere in the plasma. Finally, the resistive shell must be separated from the current carrying plasma by a region of cold tenuous plasma or, alternately, a vacuum region.

The condition (118) ensures that ideal-MHD breaks down in the outer regions of the current carrying plasma. A thick inertial layer forms whose typical width is the spacing of the rational surface from the boundary of the hot plasma. The formation of an edge inertial layer is vital to the stabilization mechanism. Note that Eq. (118) is effectively a constraint on the average rotation of the fueling ions in the inertial layer (since the fueling ions possess virtually all of the plasma inertia).

Tokamak plasmas are comparatively stable to MHD instabilities because of the rigidity

afforded to the plasma by the strong toroidal magnetic field. The distortion of the toroidal field associated with external-kink modes, whose eigenfunctions generally peak close to the edge of the plasma, is minimized when the parallel wavenumber of the instability is small at the boundary. In fact, free-boundary current-driven external-kink modes are only unstable in tokamaks when $(k_\parallel R_0)_a \ll 1$ (assuming that the current profile is reasonably peaked, and there is no edge current pedestal) [24]. This permits stabilization of the resistive shell mode in tokamaks at substantially sub-Alfvénic rotation rates (i.e. $(\omega_0 \tau_A)_{\rm crit} \ll 1$). RFPs are far more MHD unstable than tokamaks because they possess a comparatively weak toroidal magnetic field and the plasma is therefore less rigid [5]. Consequently,free-boundary current-driven external-kink modes in RFPs can be unstable when $(k_\parallel R_0)_a \sim O(1)$. Thus, in general, Alfvénic plasma rotation rates (i.e. $(\omega_0 \tau_A)_{\rm crit} \sim O(1)$) are required in RFPs in order to stabilize the resistive shell mode. This level of rotation is unattainable in practice.

Strong plasma rotation cannot by itself stabilize the resistive shell mode. In the absence of plasma dissipation the growth-rate merely asymptotes to zero as $\omega_0 \rightarrow \infty$ [11]. However, in the presence of a small amount of dissipation the growth-rate becomes negative above a finite rotation rate. The nature of the dissipation is unimportant. We have found that viscosity or resistivity acting at the plasma edge or the absorption of Alfvén waves at a toroidally coupled side-band resonant surface in the plasma are all equivalent sources of dissipation. The absorption of sound waves at a toroidally coupled side-band resonance is, presumably, also an effective source of dissipation in a finite-β plasma [20,22]. The dissipation must exceed a critical value before it is effective at stabilizing the resistive shell mode. The critical value is inversely proportional to the L/R time of the shell. This highlights the importance of making the L/R time as long as practically possible [see Fig. 9]. A thin high conductivity shell performs better than a thick low conductivity shell possessing the same overall L/R time [see Fig. 10].

Stabilization of the resistive shell mode occurs essentially because the perturbed currents

which flow at the edge of the plasma, due to the break down of ideal-MHD there, are decoupled from the eddy currents flowing in the shell by the edge plasma rotation. The strength of the coupling between these currents is inversely proportional to the spacing between the shell and the plasma boundary. Thus, as the shell moves closer to the plasma ever higher rotation rates are needed to effectively decouple the two sets of currents. Clearly, the optimum configuration is to place the shell as far away from the plasma as is consistent with the stability of the ideal external-kink mode. Modern day tokamaks tend to have relatively loose-fitting vacuum vessels (e.g. $r_{\rm w} \simeq 1.3\,a$) which permit stabilization the resistive shell mode at comparatively low plasma rotation rates. However, in the next generation of tokamaks the vacuum vessel is likely to be too remote from the plasma to significantly affect kink mode stability. In existing designs enhanced stability against external-kink modes is achieved by surrounding the plasma by a set of extremely close-fitting (e.g. $r_{\rm w} \simeq 1.05\,a$) passive stabilizing conductors. Of course, these conductors do not completely surround the plasma because of space and access requirements. The gaps between the conductors are actually beneficial (up to a point) because they reduce the coupling to the edge of the plasma. In fact, a conducting shell containing large gaps acts rather like a complete shell located somewhat further away from the plasma (see Figs. 7 and 11). Thus, it is possible for a set of extremely close-fitting passive conductors to stabilize the resistive shell mode at reasonable plasma rotation rates provided that the gaps between the conductors are sufficiently large. Of course, if the gaps are made too big then the effective shell moves too far from the plasma to stabilize the ideal mode. The optimum configuration is for the gaps to be such that the effective shell lies just inside the critical radius for stabilizing the ideal mode.

This paper concentrates on current-driven external-kink modes, rather than the more experimentally relevant pressure-driven modes, because only the former can be investigated analytically. Most of the important physics associated with the stabilization of the resis-

tive shell mode takes place close to the edge of the plasma. The free-energy of kink-modes emanates from gradients in the current and pressure profiles in the interior of the plasma. It is plausible, therefore, that the stabilization mechanism for the resistive shell mode is essentially the same for current and pressure driven modes. The one major difference between current and pressure driven modes is that the latter do not possess a unique poloidal mode-number due to the large Shafranov shift of flux-surfaces, and the consequent strong coupling of neighboring poloidal harmonics, in a high-β tokamak equilibrium [29]. However, we expect the dominant poloidal harmonic of pressure-driven external-kink modes, whose eigenfunctions tend to peak towards the edge of the plasma, to be such that $(k_\parallel R_0)_a \ll 1$ in order that the distortion of the relatively rigid magnetic field associated with the instability is kept to a minimum. Thus, it is plausible that the pressure-driven version of the resistive shell mode can be stabilized in tokamaks at substantially sub-Alfvénic rotation rates.

In conclusion, we have identified the physical mechanism which governs the stabilization of the resistive shell mode in a rotating tokamak plasma. According to our model, the fact that this mode is generally unstable in RFPs does not necessarily imply that it is unstable in tokamaks. The resistive shell mode can be stabilized in tokamaks via a combination of strong (but substantially sub-Alfvénic) edge plasma rotation and a thin, long time-constant shell which is situated neither too close to nor too distant from the plasma. It is, therefore, not completely unreasonable for advanced tokamak designs to invoke the stabilizing effect of a conducting shell in order to obtain acceptable β-limits. Nevertheless, it is by no means clear that the level of *edge plasma rotation* required to eliminate the resistive shell mode, and thereby realize the stabilizing effect of the shell, is either achievable in practice or can be maintained for any significant length of time against locked-modes, and other types of MHD activity, which are known to degrade plasma rotation in existing tokamaks [30,31].

Acknowledgments

One of the authors (RF) is indebted to Princeton Plasma Physics Laboratory Theory Division, and in particular Bill Tang, for their hospitality during his visit in the Summer of 1994. The initial inspiration for this paper was provided by the numerical results of Neil Pomphrey, Wonchull Park, and Don Monticello of PPPL.

This research was funded by the U.S. Department of Energy under contract # DE-FG05-80ET-53088.

References

[1] W.A. Newcomb, Ann. Phys. (N.Y.) **10**, 232 (1960).

[2] I.B. Bernstein, E.A. Frieman, M.D. Kruskal, and R.M. Kulsrud, Proc. Royal Soc. **A223**, 17 (1958).

[3] J.A. Wesson, in *Tokamaks* (Clarendon Press, Oxford, 1987), Ch. 6.

[4] D. Pfirsch and H. Tasso, Nucl. Fusion **11**, 259 (1971).

[5] T.C. Hender, C.G. Gimblett, and D.C. Robinson, Nucl. Fusion **29**, 1279 (1989).

[6] B. Alper, M.K. Bevir, H.A.B. Bodin, C.A. Bunting, P.G. Carolan, J. Cunnane, D.E. Evans, C.G. Gimblett, R.J. Hayden, T.C. Hender, A. Lazaros, R.W. Moses, A.A. Newton, P.G. Noonan, R. Paccagnella, A. Patel, H.Y.W. Tsui, and P.D. Wilcock, Plasma Phys. Contrld. Nucl. Fusion **31**, 205 (1989).

[7] T. Tamano, W.D. Bard, C. Chu, Y. Kondoh, R.J. La Haye, P.S. Lee, M. Saito, M.J. Schaffer, and P.L. Taylor, Phys. Rev. Letts. **59**, 1444 (1987).

[8] P. Greene, and S. Robertson, Phys. Fluids B **5**, 556 (1993).

[9] C.G. Gimblett, Nucl. Fusion **26**, 617 (1986).

[10] L.E. Zakharov, and S.V. Putvinskii, Sov. J. Plasma Phys. **13**, 68 (1987).

[11] C.G. Gimblett, Plasma Phys. Contrld. Nucl. Fusion **30**, 1853 (1988).

[12] S.W. Haney, and J.P. Freidberg, Phys. Fluids B **1**, 1637 (1989).

[13] E.J. Strait, Phys. Plasmas **1**, 1415 (1994).

[14] T.S. Taylor, E.A. Lazarus, M.S. Chu, J.R. Ferron, F.J. Helton, W. Howl, G.L. Jackson, T.H. Jensen, Y. Kamada, A.G. Kellman, L.L. Lao, R.J. La Haye, J.A. Leuer, J.B. Lister, T.H. Osborne, R. Snider, R.D. Stambaugh, E.J. Strait, and A.D. Turnbull, in *Plasma Physics and Controlled Nuclear Fusion Research 1990*, Proceedings of the 13th International Conference, Washington D.C. (IAEA, Vienna, 1991), Vol. 1, p. 177.

[15] A.D. Turnbull, T.S. Taylor, E.J. Strait, S.J. Thompson, M.S. Chu, J.R. Ferron, R.J. La Haye, L.L. Lao, R.T. Snider, B.W. Rice, D. Wròblewski, O. Sauter, M.E. Mauel, A. Popov, N. Popov, D.J. Lightly, and J.D. Williams, in *Plasma Physics and Controlled Nuclear Fusion Research 1994*, Proceedings of the 15th International Conference, Seville (IAEA, Vienna, in press).

[16] S.M. Kaye, S. Preische, N. Asakura, R. Bell, R. Fonck, A. Holland, H. Kugel, B. LeBlanc, M. Okabayashi, S. Paul, M. Reusch, N. Sauthoff, S. Sesnic, and H. Takahaschi, in *Controlled Fusion and Plasma Physics*, Proceedings of the 16th European Conference, Venice 1989 (European Physical Society, Geneva, 1989), Vol. 2, p. 561.

[17] T.H. Ivers, E. Eisner, A. Garofalo, D. Gates, R. Kombargi, M.E. Mauel, D. Maurer, D. Nadle, G.A. Navratil, M.K.V. Sankar, and Q. Xiao, in *Plasma Physics and*

Controlled Nuclear Fusion Research 1994, Proceedings of the 15th International Conference, Seville (IAEA, Vienna, in press).

[18] C. Kessel, J. Manickam, G. Rewoldt, and W.M. Tang, Phys. Rev. Letts. **72**, 1212 (1994).

[19] J. Manickam, M.S. Chance, S.C. Jardin, C. Kessel, D. Monticello, N. Pomphrey, A. Reiman, C. Wang, and L.E. Zakharov, Phys. Plasmas **1**, 1601 (1994).

[20] A. Bondeson, and D.J. Ward, Phys. Rev. Letts. **72**, 2709 (1994).

[21] D. Stork, A. Boileau, F. Bombarda, D.J. Campbell, C. Challis, W.G. Core, B. Denne, P. Duperrex, R. Giannella, L. Horton, T.T.C. Jones, E. Källne, A. Pochelon, J. Ramette, B. Saoutic, D. Schramm, J. Snipes, G. Tallents, E. Thompson, G. Tonetti, M. von Hellerman, and J. Wesson, in *Controlled Fusion and Plasma Physics*, Proceedings of the 14th European Conference, Madrid 1987 (European Physical Society, Geneva, 1989), Vol. 1, p. 306.

[22] R. Betti, and J.P. Freidberg, private communication (1994).

[23] N. Pomphrey, S. C. Jardin, J. Bialek, M. S. Chance, D.A. D'Ippolito, J.M. Finn, R. Fitzpatrick, J.L. Johnson, C.E. Kessel, J. Manickam, D.A. Monticello, J.R. Myra, M. Ono, W. Park, A. Reiman, G. Rewoldt, W.M. Tang, E.J. Valeo, L.E. Zakharov, in *Plasma Physics and Controlled Nuclear Fusion Research 1994*, Proceedings of the 15th International Conference, Seville (IAEA, Vienna, in press).

[24] J.A. Wesson, Nucl. Fusion **18**, 87 (1978).

[25] A. Aydemir, and D.C. Barnes, Jour. Comp. Phys. **59**, 108 (1985).

[26] R. Fitzpatrick, Phys. Plasmas **1**, 2931 (1994).

[27] R. Fitzpatrick, R.J. Hastie, T.J. Martin, and C.M. Roach, Nucl. Fusion **33**, 1533 (1993).

[28] R. Fitzpatrick, Phys. Plasmas **1**, 3308 (1994).

[29] F. Troyon, R. Gruber, H. Sauremann, S. Semenzato, and S. Succi, Plasma Phys. Contrld. Nucl. Fusion **26**, 209 (1984).

[30] J.A. Snipes, D.J. Campbell, T.C. Hender, M. von Hellerman, and H. Weisen, Nucl. Fusion **30**, 205 (1990).

[31] J.T. Scoville, R.J. La Haye, A.G. Kellman, T.H. Osborne, R.D. Stambaugh, E.J. Strait, and T.S. Taylor, Nucl. Fusion **31**, 875 (1991).